Mon. Not. R. Astron. Soc. **000**, 1–9 (2004) Printed 27 November 2007 (MN LATEX style file v2.2)

A Combined EIS-NVSS Survey Of Radio Sources (CENSORS) III: Spectroscopic observations

M.H. Brookes[1,2],P.N. Best[1⋆], J.A. Peacock[1], H.J.A. Röttgering[3], J.S. Dunlop[1]
[1] *SUPA†, Institute for Astronomy, University of Edinburgh, Blackford Hill, Edinburgh EH9 3HJ*
[2] *Jet Propulsion Laboratory, 4800 Oak Grove Dr., Pasadena, CA 91101, USA*
[3] *Sterrewacht Leiden, Postbus 9513, 2300 RA Leiden, the Netherlands*

27 November 2007

ABSTRACT
The Combined EIS-NVSS Survey Of Radio Sources (CENSORS) is a 1.4 GHz radio survey selected from the NRAO VLA Sky Survey (NVSS) and complete to a flux-density of 7.2 mJy. It targets the ESO Imaging Survey (EIS) Patch D, which is a 3 by 2 square degree field centred on 09 51 36.0 −21 00 00 (J2000). This paper presents the results of spectroscopic observations of 143 of the 150 CENSORS sources. The primary motivation for these observations is to achieve sufficient spectroscopic completeness so that the sample may be used to investigate the evolution of radio sources.

The observations result in secure spectroscopic redshifts for 63% of the sample and likely redshifts (based on a single emission line, for example) for a further 8%. Following the identification of the quasars and star-forming galaxies in the CENSORS sample, estimated redshifts are calculated for the remainder of the sample via the K–z relation for radio galaxies.

Comparison of the redshift distribution of the CENSORS radio sources to distributions predicted by the various radio luminosity function evolution models of Dunlop & Peacock, results in no good match. This demonstrates that this sample can be used to expand upon previous work in that field.

Key words: Surveys — galaxies: active — radio continuum: galaxies — galaxies: luminosity function

1 INTRODUCTION

The high redshift evolution of the radio luminosity function (RLF) has been speculated upon for several decades. In 1990, Dunlop & Peacock presented an investigation of both steep and flat spectrum, bright radio sources at 2.7 GHz. This work firmly established an increase, by 3 orders of magnitude, in the comoving number density of sources between redshift $\simeq 0$ and 2. At higher redshifts they presented evidence for a decline (or high redshift "cut-off") in the number density of sources with both steep and flat spectrum. However this result was dependent on the accuracy of photometric redshifts ascribed to sources from the faintest of their radio selected samples, the Parkes Selected Regions (Downes et al. 1986 and Dunlop et al. 1989). They were not able to measure the extent of the decline with redshift, only to show that the best fitting models predicted a decline in most cases. Thus, given the redshift uncertainty, it is possible that the number density of these sources doesn't actually decline until higher redshifts. The difference between a number density turnover at redshifts of 2 and 4 represents roughly 1.9 Gyrs in the history of the Universe.

Establishing the presence (or absence) of a high redshift cut-off is of interest because it provides information about the timescales over which the population of radio sources is built-up in the early Universe. This is important because the history of AGN (active galactic nuclei) activity is closely related to that of the 'normal' galaxy population. All nearby galaxies contain a supermassive black hole with mass roughly proportional to the galaxy bulge mass (Kormendy & Gebhardt 2001). Since radio-loud AGN typically reside in the most massive old elliptical galaxies (Best et al. 1998; Best et al. 2005), which host the most massive central black holes, the build-up of the radio source population offers a unique probe of the early evolution of the upper end of the black hole mass function. This is especially interesting given the possibility that the AGN themselves form part of a feedback system in which their activity affects the growth

⋆ Email: pnb@roe.ac.uk
† Scottish Universities Physics Alliance

of the black hole and host galaxy (see, for example, Springel et al. 2005 and Best et al. 2006).

The evolution of the radio-loud AGN population can also be related to that of AGN selected in other wavebands. There is a sharp cut-off in the density of optically-selected quasi-stellar objects (QSOs) at redshifts greater than 2.1 (Boyle et al. 2000, Fan et al. 2001, Wolf et al. et al. 2003, Fan et al. 2004 and references therein). The flat spectrum radio sources broadly correspond to radio–loud QSOs (as implied by Barthel 1989 and Antonucci 1993). Therefore the evolution of flat and steep spectrum radio sources may be used to test/probe the relation between radio-quiet QSOs and radio-loud QSOs (quasars), and between quasars and radio galaxies. In addition, the advent of high resolution X-ray telescopes has enabled the density of X-ray active galaxies to be studied. These sources show a variation in the redshift at which the population peaks in density as a function of luminosity (Cowie et al. 2003). At the heart of all of these studies is a desire to understand what the various types of AGN are that give rise to the sources seen at different wavelengths and how they evolve to produce the observed population behaviour.

Some progress has been made since 1990, largely in the study of flat spectrum radio sources. In 2000, Jarvis and Rawlings, found some evidence for a shallow decline, with redshift, in the number density of flat-spectrum radio sources at high redshifts (refuting an earlier claim of a sharp cut-off, in a similar sample, by Shaver et al. 1996). Subsequently, Wall et al. (2005) provided a more rigorous analysis of the behaviour of radio-loud quasars and showed that their densities are consistent with the behaviour of optical QSOs, i.e., a decline in number density at $z > 3$.

In 2001 Jarvis et al. investigated the behaviour of steep spectrum sources, finding both a shallow decline or levelling off of the number density, between $z \simeq 2.5$ and 4.5, to be consistent with the data. This sample lacked sufficient depth to precisely probe the evolution of the high redshift sources. Waddington et al. (2001) used deep radio observations to investigate luminosity function evolution and were able to discount some of the models from Dunlop and Peacock, but this sample did not have sufficient volume to improve measurements of the number density of the most powerful sources. Interestingly, they did find evidence that the space density of mJy radio sources began to turn-over at lower redshifts than that of samples with a much brighter flux-density limit. Thus, whilst it is clear that the number density of luminous steep spectrum sources increases up to redshifts beyond 2, none of these surveys, due to lack of depth or volume, has provided sufficient information about the powerful sources at redshifts beyond this.

Over the last five years the Combined EIS-NVSS Survey Of Radio Sources (CENSORS; Best et al. 2003; hereafter Paper 1) has been developed with one of the primary scientific goals being to investigate the RLF at redshifts $\gtrsim 2$. The sample contains 150 sources of radio flux density (at 1.4 GHz) greater than 3.8 mJy. Of these 137 are deemed to be complete to a flux-density limit of 7.2 mJy. As argued in Paper 1, CENSORS is of optimal depth to maximise information for the radio sources close to the break in the radio luminosity function at redshifts of $\simeq 2.5$, and is thus ideal for investigating radio source number densities at these redshifts. In order to carry out such investigations, accurate redshifts are essential for a large fraction, preferably all, of the sources in the sample. Brookes et al. (2006; hereafter Paper 2) described the follow-up imaging of the CENSORS sample, providing 92% of the sample with a clear host galaxy candidate. Only a few objects remain without any detections at all, some of which involve complications which may be solved by further follow-up in the radio. In order to achieve the high degree of spectroscopic completeness required, these host galaxy candidates have subsequently been targetted in a program of spectroscopic observations and it is these data which are described in this paper.

The layout of this paper is as follows: in Section 2 the observing strategy is described, followed by the data reduction techniques in Section 3. Section 4 presents the results of the spectroscopy, and Section 5 describes the use of the K–z relation for radio galaxies to estimate the redshifts for those sources which lack a spectroscopic redshift. Section 6 presents the redshift distribution for CENSORS and compares it to the predictions of Dunlop & Peacock (1990). Throughout this paper the following cosmological parameters are adopted: $H_0 = 70\,\mathrm{kms}^{-1}\mathrm{Mpc}^{-1}$, $\Omega_M = 0.3$ and $\Omega_\Lambda = 0.7$. Please note, if comparing to the work of Dunlop & Peacock (1990), that they assumed an Einstein–de Sitter cosmology.

2 OBSERVATIONS

The CENSORS sources detected in the I–band have magnitudes in the range $I \simeq 15$ to $I \simeq 23$ (the limit of the ESO Imaging Survey Wide survey). K–band follow up has revealed sources as faint as $K = 20.5$. Given the range in optical brightness, the following strategy (using five telescopes in eight observing runs) was adopted for spectroscopy (details of the observing runs are given in Table 1).

Multi-Object fibre Spectroscopy (MOS) using the Two Degree Field Spectrograph (2dF) on the Anglo-Australian Telescope (AAT) was employed first, as this allows the spectra of many targets to be obtained simultaneously. The 2dF consists of two spectrographs, each of which accesses 200 optical fibres which are placed on target sources, or blank sky for subtraction purposes, over a two degree field of view. The vast majority of the CENSORS field can therefore be covered in 4 pointings. Due to the small number of CENSORS sources per pointing, only one of the spectrographs was used. For each pointing, the 5400s observations were split into three 1800s exposures. In addition, a flat field and an arc were taken through the same fibre configuration, plus three 300s offset 'blank' sky frames (at three different positions) which were used to calibrate the optical throughput of the fibres. The first attempt was made in March 2000 but poor weather affected two of the pointings so these observations were repeated the following year (unfortunately, these were also weather affected).

Due to the difficulty of obtaining good sky subtraction, a 4m class telescope with fibre observations is sensitive only to the optically brightest sources, or those with bright emission lines. So, while the majority of the CENSORS sources could be targetted with 2dF, redshifts were only found for $\simeq 30\%$.

Long slit spectroscopy (LSS) was then used to target those sources without a measured redshift from the 2dF ob-

Run	Date	Telescope (Instr.)	Grism/Grating	Central λ (Å)	Resolution (Å)	Typical Seeing ($''$)	Strategy
1a	20000301	AAT (2dF)	270R	6503	10	1.5	4 pointings of 3*1800s
1b	20010307	AAT (2dF)	270R	6503	10	1.5	2 pointings of 3*1800s
2	20020212 - 15	VLT (FORS1)	300V	5850	11.1	0.7-1.5	Up to 3 x 20 min exposures.
3	20030204 - 08	ESO 3.6m (EFOSC2)	Gr#6	5965	12.9	1.0	Up to 3 x 30 min exposures.
4	20030226 - 28	VLT (FORS1)	300V	5850	11.1	0.7-1.5	Up to 3 x 30 min exposures.
5	20050206	VLT (FORS1)	300V	5850	11.1	0.7-1.5	600-1800s exposures
6	20050413	WHT (ISIS)	R316R/R158B	6500/3600	12/13	1.4	900s
7	20060223	VLT (FORS1)	300V	5850	11.1	0.7-1.5	Up to 3 x 30 min exposures
8	20060226-28	VLT (FORS2)	300I	8600	11.3	1.0-1.5	1 to 4 x 20 min exposures

Table 1. Details of the spectroscopic observations for CENSORS.

servations. The ESO 3.6m telescope at La Silla was used in 2003 to target intermediately-bright sources (in the optical) with a $1.5''$ slit. Up to three exposures of 30 minutes each were taken, with the later exposures being stopped if a redshift was immediately apparent in the first data.

The optically-faintest sources (generally those which were only detected in the K–band) were targetted with FORS1 on the 8m class ESO Very Large Telescope (VLT), in 2002, 2003 and 2006, using a $1''$-$1.5''$ slit. Further service mode observations were made in 2005 using the VLT and the William Herschel Telescope (WHT). A subset of sources for which no redshift was obtained were targetted at redder wavelengths with FORS2 in 2006. Full details of the observations are provided in Tables 1 and A1.

3 DATA REDUCTION

3.1 Multi-object spectroscopy

The process of 2dF data reduction involves: removal of bad pixels and bias subtraction; extraction of the spectra from the raw frame; wavelength calibration with reference to the extracted arc observation; fibre throughput estimation and correction via offset sky images; sky subtraction, using the median sky as calculated from sky fibres; and, finally, combination of multiple exposures. No flux calibration was available for these data.

The 2dF data reduction pipeline (2dFdr; see `http://www.aao.gov.au/2df/software.html`) was used for the initial steps of this process, up to and including the fibre extraction. It was not used thereafter, because the pipeline results produced poor quality spectra, in which only the brightest sources could be identified spectroscopically. Many of the spectra were over or under subtracted in relation to the sky spectrum. This over-/under-subtraction varied with position on the extracted image indicating that it was likely due to variation of the sky background over the field of view. It should be noted that this is a particular problem for galaxies such as those in CENSORS because they are so faint, making sky subtraction errors particularly problematic.

To avoid this problem, an improved sky subtraction code was developed. The three pipeline-produced fibre-extracted images (which each contain about 200 rows corresponding to the fibres observed) for both the target and the offset sky were combined in IRAF with cosmic ray rejection. The combined offset sky image was then used to determine the relative fibre throughput, and the combined target frame was corrected for this. Sky subtraction was then carried out by assuming that the sky varied, with fibre number, as a low order polynomial (of order 2) plus a distortion, introduced by the throughput and scattered light term. The sky fibre counts were fitted as a function of fibre number for all wavelengths and subtracted from all fibres. The median of the residual background (taken from the sky subtracted sky fibres) was then subtracted, for all pixels in wavelength, to account for remaining distortion. This dramatically improved the background subtraction for the majority of the spectra.

There remained twelve CENSORS sources for which there was significant continuum detected, but insufficient signal-to-noise to assign a redshift. For these sources the sky subtraction was repeated, instead using only those sky fibres identified to be located in a similar region of the sky as the target. This target-specific reduction was a lengthy procedure, but did improve the sky subtraction and yielded two further redshifts.

3.2 Long Slit Spectroscopy

The data reduction technique was identical for all observations and proceeded, using the IRAF data reduction package, as follows. The raw 2D images were bias subtracted and flat fielded. The sky background was fitted and subtracted and the spectrum was extracted. Flux calibration information was extracted from a flux standard and applied to each target, and wavelength calibration was performed on the basis of an arc lamp observation. The flux standards used varied for different observing runs and include: Hiltner 600, Feige 56, LTT2415 and GD108. The spectra were extracted with apertures of width in the range 0.9 - 2.4 arcsec; the smaller extraction apertures were used for those sources

with very little continuum for which emission lines were the only features. Subsequently, residuals from the subtraction of strong sky lines were replaced by an interpolation of the surrounding continuum in order to ease interpretation of the spectra.

4 SPECTROSCOPIC REDSHIFTS

The method for identifying redshifts followed these steps:

- If there were multiple emission lines, the ratios of their wavelengths were used to identify them and derive an approximate redshift.
- The spectrum was then analysed in an IDL script which measured the properties of all emission lines (and provided a more accurate measurement of the redshift). The properties measured for each emission line were: the full width at half-maximum, which may be used as a diagnostic for finding quasars; the emission line flux (for calibrated spectra); the equivalent width. The line properties are given for the rest-frame in Table A1. Note that because the Ly α line can have a distorted shape due to intervening matter absorption, giving rise to an incorrect redshift estimate, this line is excluded from the redshift determination.
- Where there was only a single emission line, this line was generally assumed to be one of the typically bright emission lines, e.g. Ly α, MgII or [OII], as these are the only ones which one might expect to find alone. MgII was easily distinguished by its broad shape. Ly α and [OII] were distinguished by considering the K–band magnitude and the redshift expected from the K–z relation for radio galaxies.
- Where there were no emission lines, but there were absorption features, the positions were measured in IRAF, using a Gaussian fit, in order to establish the redshift.
- In many spectra which did not lead to a redshift measurement via emission lines or absorption features, continuum emission was nevertheless detected. In some cases it was sufficiently strong that cross-correlation with a template galaxy spectrum was attempted to see if a redshift might be recovered. This was tried for three sources (CENSORS 34, 128 and 148), using the elliptical galaxy template of Kinney et al. (1996) in the 'fxcor' package of IRAF. Since all of these candidates have 2df spectra which have not been flux calibrated, both the galaxy spectra and the template were divided by their smoothed spectra to improve the cross correlation of features only. However, no redshifts were recoverable.

The results of these observations are presented in Table A1. In order to have all the CENSORS spectroscopic information in one place, this table presents the status of all CENSORS sources, including those which have not yet been targetted and also those for which no redshift was measured but an estimate has been made (see Section 5). A column identifying which sources are believed to be starbursts or quasars is also included (again, see Section 5). Where spectra were successfully used to find a redshift, they are plotted in Appendix C. Uncertainties in the assigned redshift are also noted in Table A1 and justification of the choice of redshift (where necessary) is discussed source by source in Appendix B.

It is finally noted that CENSORS 58 is located very close to a bright galaxy (see Paper 2), prohibiting identification and spectroscopic follow-up. This source is removed from the sample for the analysis presented in the remainder of this paper. Since this is a random selection, it is not believed that removing CENSORS 58 from the sample will systematically affect the results.

5 REDSHIFT ESTIMATION VIA THE K–Z RELATION FOR RADIO GALAXIES

In order to use this sample to investigate the evolution of the radio luminosity function, a complete list of flux densities and redshifts is required. Paper 1 presents 1.4 GHz flux densities for CENSORS and the current work presents the spectroscopic redshifts. In this section, redshift estimates are described for the CENSORS sources which remain without a spectroscopic redshift.

These redshift estimates were made via the K–z relation for radio galaxies. K–band observations of radio galaxies are dominated by emission from the old stellar population. Since near-IR emission does not change as rapidly with evolution of the stellar population as the shorter wavelength emission, and radio galaxy hosts form a fairly homogeneous sample of objects, a tight relation exists for radio galaxies between K–band magnitude and redshift (Lilly & Longair 1984, Eales & Rawlings 1996, Best et al. 1998).

The K–z relation for radio galaxies is known to vary slightly between samples of different flux-density limits. This has been shown by a number of studies comparing the 3CRR, 6C and 7C radio surveys (e.g. Eales & Rawlings 1996, Jarvis et al. 2001, Inskip et al. 2002 and Willott et al. 2003). In Paper 2 it was shown that the CENSORS sample obeys a K–z relation similar to that of the 7C (7C is the faintest radio survey of those listed above and CENSORS is fainter again) and this relationship has therefore been used to estimate redshifts for the radio galaxies in the CENSORS sample.

5.1 Identifying Starburst galaxies and Quasars in CENSORS

The K–z relation is applicable only to radio galaxies (for which the K–band emission is dominated by an old elliptical galaxy). Therefore it is necessary to identify any starburst galaxies or quasars in the CENSORS sample before it can be used for redshift estimation.

5.1.1 Starburst galaxies

In very deep radio surveys, star-forming galaxies begin to dominate the radio source population (e.g. Seymour et al. 2004). Jackson & Wall (1999) investigate a dual population scheme for AGN radio sources using the two radio morphologies, FRI and FRIIs, as their basis. They predict that around 10% of radio sources at the flux density limit of the CENSORS survey may be starburst galaxies. Therefore CENSORS may contain a significant number of these sources.

A list of candidate starburst galaxies was produced from the CENSORS sample. All sources with spectroscopic redshift greater than 0.5 or radio luminosities greater than

2×10^{24}W Hz^{-1} were removed since the starburst population only dominates the radio galaxies at low luminosities (2×10^{24} was chosen based on the local luminosity functions for AGN and star forming galaxies, as being where the space density of star forming galaxies is about two orders of magnitude below that of AGN; Sadler 2002). Of the remaining sources, those with $K > 16.5$ were removed as these are highly likely to be at redshifts greater than 0.5 (according to the K–z relationship; described in Section 5.2) plus any sources with jets in their radio structure. This left nine candidate star forming galaxies.

A useful way to distinguish star forming galaxies from AGN is to use a diagram which compares the line flux ratios of [OIII] 5007/Hβ and [NII]6583/Hα (hereafter referred to as a BPT diagram; Baldwin et al. 1981; Kauffmann et al. 2003) because on this plot AGN and star-forming galaxies fall in different regions. Three sources can be investigated in this way.

CENSORS 18 has $\log_{10}$([OIII]5007/Hβ) $= -0.281$ and $\log_{10}$([NII]6583/Hα) $= 0.254$, whereas for CENSORS 149 $\log_{10}$([OIII]5007/Hβ) $= -0.237$ and $\log_{10}$([NII]6583/Hα) $= -0.595$. Thus CENSORS 149 falls on the star formation track of Fig. 1 of Kauffmann et al. (2003) and is a star-forming galaxy, whereas CENSORS 18 lies in the LINER region. CENSORS 18 also has broad lines in its spectrum, confirming its AGN classification. CENSORS 95 has both Hα and [N II] detected in its spectrum, though no [O III] or Hβ (suggesting it is may be a heavily dust reddened source). However the ratio $\log_{10}$([NII]6583/Hα) $= -0.602$, so this source is clearly more consistent with being a star-forming galaxy.

Four more starburst candidates are CENSORS 93, 108, 140 and 148. None of these sources show the appropriate emission lines in their spectra to use the BPT diagram. However, it is possible to classify them on the basis of their lack of an [O II] detection.

Barbaro & Poggianti (1997) provide a relation between the [O II] line luminosity and the (upper limit to the) star formation rate. Condon & Yin (1990) provide a relation between the radio luminosity and star formation rate of star-forming galaxies. Combining these results the relation between [O II] line emission and radio luminosity (assuming star formation as the origin) is (cf. Best et al. 2002):

$$S_{1.4\,\mathrm{GHz}}[\mu Jy] \sim 18.4 \left(\frac{f_{[\mathrm{OII}]}}{10^{-16} ergs^{-1} cm^{-2}} \right) (1+z)^{-0.8}, \quad (1)$$

where $f_{[\mathrm{OII}]}$ is the [O II] line flux. This is plotted in Fig. 1 for a source at $z = 0.24$ (similar to the redshifts of CENSORS 108 and 140, though the variation is not significant for the other sources).

The 1.4 GHz flux for a given line luminosity that is expected for AGN may also be estimated. Willott et al. (1999) provide a relation between 151 MHz radio luminosity and [O II] line luminosity for radio-loud AGN. Following Best et al. (2002), this can be scaled to 1.4 GHz assuming a spectral index of $\alpha = 0.8$, and extrapolated to low flux densities, giving:

$$S_{1.4\,\mathrm{GHz}}[\mu Jy] \sim 4.7 \times 10^4 \left(\frac{f_{[\mathrm{OII}]}}{10^{-16} ergs^{-1} cm^{-2}} \right)^{1.45}. \quad (2)$$

Thus, the upper limit for emission line flux for these four candidates can be compared to the radio luminosity to investigate its origin. Although the 2dF spectra for CENSORS 93, 108, 140 and 148 are not flux calibrated, a limit on the line flux may be estimated by combining the V–band continuum flux density (from the EIS broad band magnitude) with the upper limit to the line equivalent widths. The V–band is close enough in wavelength to the redshifted line for this to be reasonable.

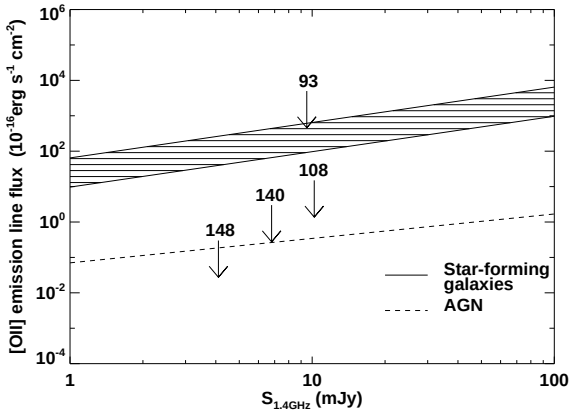

Figure 1. The relationship between [O II] line flux and radio luminosity for star-forming galaxies and AGN, for a redshift of 0.24. This redshift is chosen as it is similar to those of CENSORS 108 and 140, however the difference for the redshifts of the other sources is not significant. The shaded region shows the effect of 2 orders of magnitude of dust extinction on the star-forming galaxies. The dashed line plots the expected relation for AGN. The limits for CENSORS 108, 140, 148 clearly indicate that they are AGN. Although the limit for CENSORS 93 is consistent with either a star-forming galaxy or an AGN, its spectrum is very typical of an old, red elliptical.

Fig. 1 plots the limiting [O II] line fluxes against their radio fluxes and the theoretical relations for star-forming galaxies and AGN. The shaded region shows the effect of 2 magnitudes of dust extinction on the star-forming galaxies. The limits for CENSORS 108, 140 and 148 are clearly closer to the dashed AGN line. The limit for CENSORS 93 is consistent with the star-forming region of the plot. However, the spectrum of CENSORS 93 in Figure C1, shows that it is typical of an old, red elliptical galaxy and not a star-forming galaxy. Therefore all of these candidates are considered to be AGN.

The final two star-forming candidates, CENSORS 124 and 146, are both very low redshift. Their radio flux densities in the VLA BnA array observations are very much lower than those in the NVSS, indicating that they are diffuse sources. Such diffuse radio emission is more often associated with starbursts and not AGN. In addition the radio luminosities of these sources are $\simeq 10^{22}$ W Hz^{-1} at 1.4 GHz, making them more likely to be star-forming galaxies rather than AGN.

The final list of radio sources due to star formation in the CENSORS sample is: CENSORS 95, 124, 146, 149.

5.1.2 Quasars

The SExtractor parameter S/G is provided by the EIS catalogue, and varies from 0.0 to 1.0, 1.0 being the most point-like. In Paper 1, 11 sources were identified as possible quasars on the basis of their stellaricity measure being $S/G > 0.9$. Some sources with a slightly lower stellaricity were also included as possible quasars on account of their blue colour ($S/G > 0.6$ and $B - I < 1$). From the spectra presented in this work, quasars may be identified by having broad emission lines (broader than the $\simeq$ $1000\,\mathrm{km\,s^{-1}}$ line width of radio galaxies). Sources are considered candidates for quasars if they have permitted lines, other than Lyα (which can be broadened by resonant scattering), which are significantly broader than $1000\,\mathrm{km\,s^{-1}}$.

Combining these two methods, CENSORS 6, 7, 10, 11, 29, 39, 44, 48, 92 and 116 are classified as quasars by both methods, and are considered certain quasars. CENSORS 63, 82, 100, 126, 129 are classified as quasars from the imaging data, but do not show the broad emission lines, whilst CENSORS 18, 37, 38, 49, 52, 92, 114, 129, 135 are spectroscopic quasar candidates but were not classified as quasars from the imaging data. These additional quasar candidates were considered individually (as described in the notes on individual sources which are presented in Appendix B), and CENSORS 37, 38, 114 and 135 were added to the list of quasars.

In total, the quasars within the CENSORS sample are CENSORS 6, 7, 10, 11, 29, 39, 44, 48, 63, 82, 92, 100, 116, 126.

5.2 Estimating redshifts using the K–z relationship for radio galaxies

In Paper 2, it was shown that the K-z relationship, based upon the 7C radio selected sample from Willott et al. (2003) is applicable to CENSORS. In order to estimate the redshift from the K-band magnitude, the fit of K as a function of z (as the K-z relationship is traditionally expressed), should not simply be mathematically inverted as that leads to over-predictions of the redshifts of faint K-sources (due to the small number of high redshift sources). Rather, the relation should be re-fitted using K as the independent variable. This is discussed in more detail in Cruz et al. (2007).

A second order polynomial, $\log_{10} z(K)$, was produced by fitting to the 7C data via a least squares method, providing the following equation:

$$\log_{10} z = 0.003K^2 + 0.11K - 2.74 \qquad (3)$$

The scatter, σ_{7C}, about the predicted $\log_{10} z$ for the 7C sources is 0.14.

This relation is applied to the K–band magnitudes measured for those CENSORS sources without spectroscopic redshifts in order to derive a redshift estimate; the redshift estimate is then used to correct the photometry to the standard aperture used to define the K–z relationship (see Paper 2 for details) and the process is repeated iteratively. The aperture chosen for this calculation was the one which, by eye whilst executing the photometric measurements, covered the most source emission without being unnecessarily large (in order to keep photometric errors as low as possible). Where no detection was made in the K–band, the 2-σ limiting magnitude, based on a $1''$ radius aperture, was used to derive a redshift estimate as described above. This estimate was then reduced to a 95% confidence lower limit, based upon the scatter in $\log_{10} z$ in the K–z relation. The results of the redshift estimation are presented in Table 1.

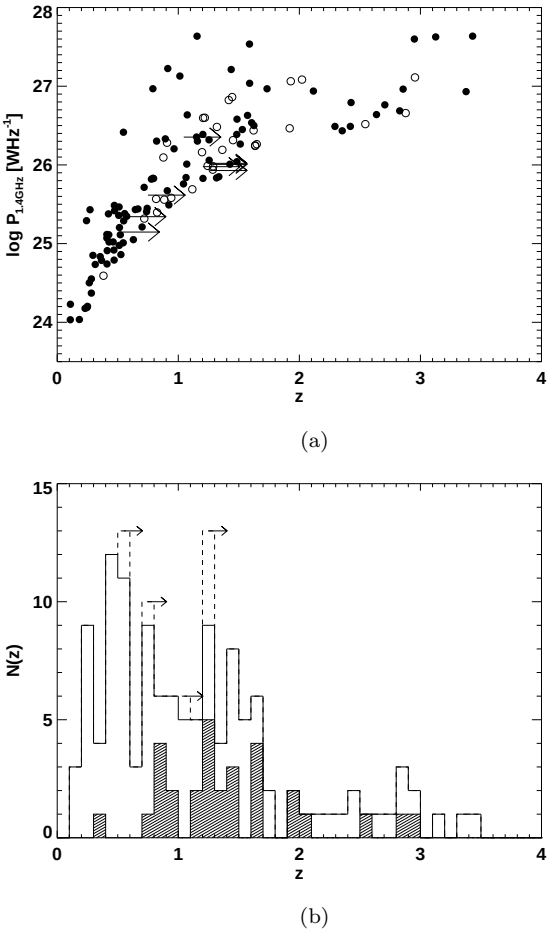

(a)

(b)

Figure 2. (a) The coverage of the radio-luminosity–redshift plane provided by the CENSORS sample. Closed circles indicate spectroscopic redshifts (including those with single line redshift assignments) and open circles indicate estimated redshifts on the basis of the K– or I–z relations. Arrows indicate 95% confidence, lower limits to redshifts for sources with no spectroscopic redshift and no K–band detection as described in the text. Note that if these sources were at higher redshifts, their luminosities would also increase. (b) The redshift distribution for the CENSORS sample. The hashed area represents those sources with redshifts estimated from the K–z relation for radio galaxies. The unfilled region represents spectroscopic redshifts and the dashed/arrowed region represents lower limits to redshifts based upon the K–z relation.

5.3 I–z relationship for CENSORS 112

The FORS1 spectrum of CENSORS 112 has faint blue continuum, but no features. A K–band magnitude is not available for this source, so it is not possible to use the K–z relationship to estimate its redshift. A redshift may be estimated using the I–z relationship, following Best et al. (2003). Using this relation the redshift for CENSORS 112 is estimated to be $z = 1.75$.

Total Sources	149
Total targetted	143
Literature redshifts	2
Total secure redshifts†	81
Less secure redshifts†	2
Well justified single line redshifts	11
Less secure single line redshifts	9

Table 2. A summary of the results of spectroscopic observations of CENSORS. † Not including single line redshifts.

MODEL	N° Sources	Data 1	Data 2
1	122	0.35	0.61
2	122	1×10^{-6}	2×10^{-4}
3	148	0.005	9×10^{-4}
4	141	0.16	0.09
5	139	0.07	0.15
PLE	131	3×10^{-6}	1×10^{-4}
LDE	115	2×10^{-5}	7×10^{-4}

Table 3. The number of sources predicted to the CENSORS flux density limit (compared to 134 observed) for each of the DP90 models, and the probabilities, according to a K-S test, that the redshift distribution of those sources could be drawn from the same source distribution as the CENSORS data. Here 'Data 1' refers to the best estimated redshift distribution in which all estimated redshifts are assumed correct. In 'Data 2' each source which has an estimated redshift has had the single 'best' value of estimated redshift (used in 'Data 1'), replaced with a spread of values which integrate to unity as described in the text. Note that the K-S test probability gives only the probability that the normalised distributions are the same, and does not address the differences in the total numbers of sources predicted.

6 THE CENSORS REDSHIFT DISTRIBUTION

6.1 A summary of the current redshift status of the CENSORS sources

Excluding CENSORS 58 there are 149 sources, of which 143 have been spectroscopically targetted. Of the 6 sources not targetted, 2 have redshifts available from NED and the remaining 4 were not observed due to poor weather or lack of observing time. The sample as a whole is 71% spectroscopically complete and this figure does not change if only the 136 sources complete to a flux-density of 7.2 mJy at 1.4 GHz are considered. A break down of the relative certainties of the redshifts ascribed is given in Table 2.

Of those sources without spectroscopic redshifts, one source has a redshift estimated from the I-z relation, and all but 9 more have redshifts estimated from the K-z relation. For the remainder, a non-detection in the K band offers a lower limit to the redshift. Table A1 lists the final redshift assigned to each source and a comment on the origin of the redshift estimate. This table includes all spectroscopic and estimated redshifts for CENSORS. In the column listing the redshifts, the symbols '**?**' and '**s**' are used to clearly identify those redshifts which are considered to be less secure and/or derived on the basis of a single line.

On the basis of the presented spectroscopic and estimated redshifts, the radio luminosity–redshift plane and redshift distribution are plotted for the CENSORS sample in Fig. 2. This figure and, henceforth, the discussion, is limited to the 134 sources which are complete to 7.2 mJy at 1.4 GHz and whose radio emission is not due to star formation. As expected, the spectroscopic completeness of the sample is greater at low redshifts, say $z \lesssim 1.1$ at which it is $\simeq$ 82%, compared with higher redshifts at which it is reduced to $\simeq$ 56% (assuming the redshift estimates are roughly correct). This is to be expected as it is the sources likely to be at high redshifts that are more likely to be without a detection of the host galaxy. In addition, measuring redshifts of galaxies which lie between of 1.1 and 2.2 (the redshift desert) is difficult as neither the [OII] or Lyα lines are present in the spectrum.

6.2 Comparison with the Dunlop and Peacock models

The development of the CENSORS sample was primarily motivated by the need to provide increased coverage of the luminosity-redshift plane to improve our knowledge of the cosmological evolution of the radio luminosity function. Now that the required redshift information has been assembled, a preliminary assessment of the potential impact of this sample on the determination of the evolving RLF can be undertaken. One way to do this is to compare the redshift distribution of the CENSORS sample with that predicted by existing models of the RLF. The most appropriate comparison is with the best-fit models of Dunlop & Peacock (1990). Not only is this work the most complete of its kind, but it is also based upon high frequency data (2.7 GHz) and may be used to make predictions for the CENSORS sample with the least errors introduced by making the correction to 1.4 GHz.

In Dunlop & Peacock (1990), five free-form models were fitted to the data available at the time. Free form model 1 (FF1) describes the number density as a series expansion of $0.1(\log P - 20)$ and $0.1z$. FF2, 3, 4, and 5 are similar but explore the effect of imposing cut-offs at high luminosity (FF2) or redshift (FF5), changing the nature of the coordinates in luminosity and redshift (FF3), and terminating the integration of the luminosity-redshift plane at $z = 5$ instead of $z = 10$ (FF4). In addition two models with more general assumptions regarding the evolution were also fitted. These were pure luminosity evolution and luminosity–density evolution. Dunlop & Peacock (1990) model the flat and steep spectrum radio sources separately. Since these populations cannot yet be separated within the CENSORS sample, it is the combined steep and flat spectrum predictions from Dunlop & Peacock (1990) which are used in the comparison.

Table 3 provides the probabilities, based upon the K–S tests, that a given model could be produced by the same source distribution as the data. Here 'Data 1' is used to describe the best estimated redshift distribution. This is essentially the distribution plotted in Figure 2(b) however the sources for which redshifts are based upon K–band limits are placed at their best redshift estimate, as calculated by Equation 3, as opposed to the 95% confidence lower limit to their redshift.

Models 1, 4 and 5 have a >5% chance of matching the observed (normalised) redshift distribution, with other models strongly ruled out. However, model 1 badly underpredicts the number of sources at these faint radio flux densities, and we are left to conclude that models 4 and 5 provide the best description of the data. Interestingly, this was also the finding of Waddington et al. (2001), although the actual

agreement with the redshift distribution of their sample was somewhat better than found here.

Figure 3(a) presents the comparison graphically and can be usefully compared with Figure 9 from Waddington et al. (2001). It plots the cumulative redshift distribution, N($< z$), of CENSORS (solid circles) as compared with the best fitting models of Dunlop & Peacock (1990). The shaded region indicates the error as calculated by finite number statistics. It is clear that none of the Dunlop & Peacock (1990) models are a really good fit to the data over all redshifts. In this plot the distributions are plotted in terms of the absolute number of sources, thus highlighting where the models may have a reasonable shape but predict the wrong number of sources (the K–S test assesses only the maximum difference between the normalised distributions). However this comparison is somewhat confused by the assumption in this figure that the distribution for the data may be represented by the estimated redshifts without account for the uncertainty.

In order to account for the uncertainty in the distribution a smoothed version (Data 2) has been produced. In this smoothed distribution, the K–z redshifts are replaced by a Gaussian distribution about the best estimated redshift of the width $\sigma = \sigma_{7C}$ (the width of the scatter of the K–z relation about $\log z$). The total contribution is one source but spread over a range in redshifts. In a similar way the K–z estimated redshifts that are based upon limiting K–band magnitudes are replaced by a source which is spread $\sigma = \sigma_{7C}$ to lower redshifts and $\sigma = 2\sigma_{7C}$ to higher redshifts than the best estimated redshift from Equation 3. Note that adopting a 2σ spread to high redshifts is somewhat arbitrary, but changing this to 4σ did not affect the conclusions. CENSORS 112, for which the I–z relation is used, has been treated in the same way as the K–z sources.

Figures 3(b) and (c) plot this smoothed distribution (filled circles) in comparison to the Dunlop & Peacock (1990) models. The shaded regions show the change if all K-band estimated redshifts are moved up or down by 1-sigma. These figures show that the uncertainty in the distribution is dominated by the scatter in the K–z relation and that more spectroscopic redshifts, or more accurate photometric redshift estimates, are required in order to tie down the shape of the distribution precisely. The fact that none of the Dunlop & Peacock (1990) models provides a very good fit to the CENSORS data demonstrates that the sample is probing a region of parameter space which was not available before. CENSORS may therefore play an important role in expanding on previous work.

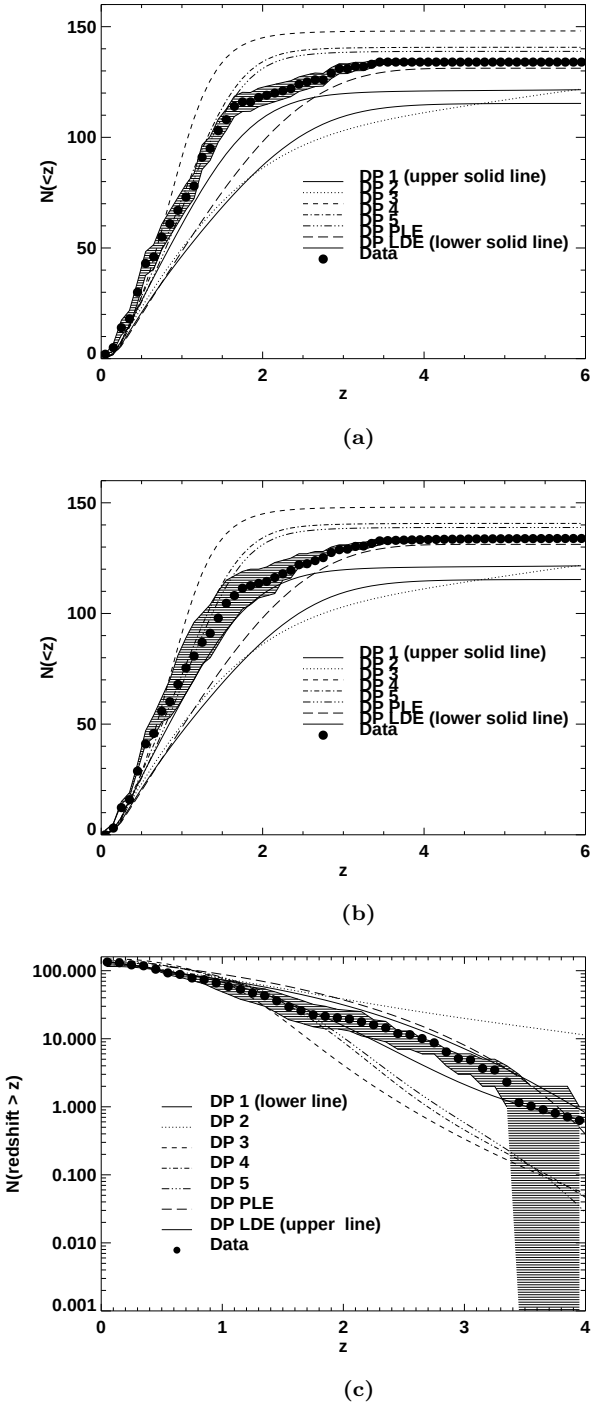

Figure 3. The cumulative redshift distributions, N($< z$), of the CENSORS sample.The shaded regions indicate the uncertainty as calculated by finite number statistics, in **(a)**, and the uncertainty due to the 1–σ spread in the K–z relation about the estimated redshifts, in **(b)**. **(c)** plots the redshift distribution, N($> z$), which highlights the differences between the smoothed data and the models at high redshifts.

7 SUMMARY

Of 150 CENSORS sources, 143 have been spectroscopically targetted using the AAT, VLT, WHT and ESO 3.6m telescopes. These observations, plus results from the literature, have resulted in secure spectroscopic redshifts for 56% of the sample based upon two or more emission lines or absorption features. In addition 22 sources have less certain redshifts. Of these 20 are based upon a single emission line, but 11 are considered secure redshifts when photometry and the lack of other bright lines are taken into account. Including all of these redshifts, the sample is 71% spectroscopically complete.

Quasars and starbursts have been identified in the sample, thus allowing redshift estimation, on the basis of the K–z relation for radio galaxies (derived from the 7C radio survey in Paper 2), for those sources without a spectroscopic redshift. For CENSORS 112, an estimate based on an I–z relation was made.

The resulting redshift distribution has been compared to the predictions of the best fitting models from Dunlop & Peacock (1990). None of these models provides a convincing match to the data. These results demonstrate that this new sample probes a region of radio luminosity and redshift space which was not available at the time of the Dunlop & Peacock (1990) investigation. Since that investigation has been the most complete to deal with all radio sources selected at relatively high frequencies, it is clear that a new study into the evolution of radio sources is timely.

ACKNOWLEDGEMENTS

MHB is grateful for the support of a PPARC research studentship, and JAP is grateful for the support of a PPARC Senior Research Fellowship. PNB thanks the Royal Society for generous financial support through its University Research Fellowship scheme. Observations were made using the Anglo-Australian Telescope, the William Herschel Telescope, the ESO Very Large Telescope at the Paranal observatory (69.A-0047, 71.A-0622, 76.A-0745) and the ESO 3.6m telescope at La Silla observatory (70.A-0225)

REFERENCES

Antonucci R., 1993, ARA&A, 31, 473
Baldwin J. A., Phillips M. M., Terlevich R., 1981, PASP, 93, 5
Barbaro G., Poggianti B. M., 1997, A&A, 324, 490
Barthel P. D., 1989, ApJ, 336, 606
Best P. N., Arts J. N., Röttgering H. J. A., Rengelink R., Brookes M. H., Wall J., 2003, MNRAS, 346, 627
Best P. N., Kauffmann G., Heckman T. M., Brinchmann J., Charlot S., Ž. Ivezić White S. D. M., 2005, MNRAS, 362, 25
Best P. N., Kaiser C. R., Heckman T. M., Kauffmann G., 2006, MNRAS, 368, L67
Best P. N., Longair M. S., Röttgering H. J. A., 1998, MNRAS, 295, 549
Best P. N., van Dokkum P. G., Franx M., Röttgering H. J. A., 2002, MNRAS, 330, 17
Boyle B. J., Shanks T., Croom S. M., Smith R. J., Miller L., Loaring N., Heymans C., 2000, MNRAS, 317, 1014
Brookes M. H., Best P. N., Rengelink R., Röttgering H. J. A., 2006, MNRAS, 366, 1265
Condon J. J., Yin Q. F., 1990, ApJ, 357, 97
Cowie L. L., Barger A. J., Bautz M. W., Brandt W. N., Garmire G. P., 2003, ApJl, 584, L57
Cruz M. J., Jarvis M. J., Rawlings S., Blundell K. M., 2007, MNRAS, 375, 1349
Downes A. J. B., Peacock J. A., Savage A., Carrie D. R., 1986, MNRAS, 218, 31
Dunlop J. S., Peacock J. A., 1990, MNRAS, 247, 19
Dunlop J. S., Peacock J. A., Savage A., Lilly S. J., Heasley J. N., Simon A. J. B., 1989, MNRAS, 238, 1171
Eales S. A., Rawlings S., 1996, ApJ, 460, 68
Fan X. e. a., 2001, AJ, 121, 54
Fan X. e. a., 2004, AJ, 128, 515
Inskip K. J., Best P. N., Longair M. S., MacKay D. J. C., 2002, MNRAS, 329, 277
Jackson C. A., Wall J. V., 1999, MNRAS, 304, 160
Jarvis M. J., Rawlings S., 2000, MNRAS, 319, 121
Jarvis M. J., Rawlings S., Eales S., Blundell K. M., Bunker A. J., Croft S., McLure R. J., Willott C. J., 2001, MNRAS, 326, 1585
Jarvis M. J., Rawlings S., Willott C. J., Blundell K. M., Eales S., Lacy M., 2001, MNRAS, 327, 907
Kauffmann G., Heckman T. M., Tremonti C., Brinchmann J., Charlot S., White S. D. M., Ridgway S. E., Brinkmann J., Fukugita M., Hall P. B., Ivezić Ž., Richards G. T., Schneider D. P., 2003, MNRAS, 346, 1055
Kinney A. L., Calzetti D., Bohlin R. C., McQuade K., Storchi-Bergmann T., Schmitt H. R., 1996, ApJ, 467, 38
Kormendy J., Gebhardt K., 2001, in AIP Conf. Proc. 586, "20th Texas Symposium on Relativistic Astrophysics", p363
Leggett S. K., Allard F., Berriman G., Dahn C. C., Hauschildt P. H., 1996, ApJS, 104, 117
Lilly S. J., Longair M. S., 1984, MNRAS, 211, 833
Mathewson D. S., Ford V. L., 1996, ApJS, 107, 97
Mathewson D. S., Ford V. L., Buchhorn M., 1992, ApJS, 81, 413
Sadler E. M. e. a., 2002, MNRAS, 329, 227
Seymour N., McHardy I. M., Gunn K. F., 2004, MNRAS, 352, 131
Shaver P. A., Wall J. V., Kellermann K. I., Jackson C. A., Hawkins M. R. S., 1996, Nature, 384, 439
Springel V., Di Matteo T., Hernquist L., 2005, MNRAS, 361, 776
van Ojik R., Röttgering H. J. A., Miley G. K., Bremer M. N., Macchetto F., Chambers K. C., 1994, A&A, 289, 54
Waddington I., Dunlop J. S., Peacock J. A., Windhorst R. A., 2001, MNRAS, 328, 882
Wall J. V., Jackson C. A., Shaver P. A., Hook I. M., Kellermann K. I., 2005, A&A, 434, 133
Willott C. J., Rawlings S., Blundell K. M., Lacy M., 1999, MNRAS, 309, 1017
Willott C. J., Rawlings S., Jarvis M. J., Blundell K. M., 2003, MNRAS, 339, 173
Wolf C., Wisotzki L., Borch A., Dye S., Kleinheinrich M., Meisenheimer K., 2003, A&A, 408, 499

APPENDIX A: DETAILS OF THE SPECTROSCOPIC OBSERVATIONS AND RESULTS

Table A1 provides full details of the spectroscopic observations, the resulting spectra and line properties, and the redshift estimates for sources without spectroscopic redshifts.

Table A1.

CEN	RA	DEC	Run	Exp. Time (s)	Slit PA	Line	$\Lambda_{\rm obs}$ Å	$10^{-16}\times$ Flux erg/s/cm^2	$\Delta v_{\rm FWHM}$ kms^{-1}	W	z	Δz	z_K	Note
1	09 51 29.22	−20 50 30.68	1,**3**	3600	+111	CIII]	4107	3.62 ± 0.50	930 ± 403	72 ± 19	1.155	0.001		S
						NeIV	5222	1.71 ± 0.22	858 ± 345	24 ± 4				
						[NeV]	7382	2.08 ± 0.26	260 ± 187	40 ± 6				
						[OII]	8031	4.23 ± 0.29	-	75 ± 28				
2	09 46 50.22	−20 20 44.45	**2**	3600	+139	[OII]	7130	0.38 ± 0.05	457 ± 266	-	0.913**s**	-		S,N
3	09 50 31.32	−21 02 44.18	1,**3**	3600	+116	[OII]	6672	1.51 ± 0.18	1222 ± 345	61 ± 11	0.790	0.001		S
4	09 49 53.26	−21 56 19.90	**1**		-	[NeV]	6900	-	300 ± 200	-	1.013	0.0003		S, N
						[OII]	7503	-	600 ± 200	-				
5	09 53 44.47	−21 36 01.75	1,**3**	1800	+0	Lyα	4361	24.2 ± 2.34	1000 ± 200	285 ± 50	2.588	0.002		S
						NV	4450	-	-	-				
						HeII	5884	2.74 ± 0.25	800 ± 200	52 ± 9				
						CIII]	6846	0.71 ± 0.122	700 ± 400	24 ± 6				
6	09 51 43.56	−21 23 58.00	**5**	1200	-	MgII	4333	142 ± 16	4182 ± 369	369 ± 4	0.547	0.0004		S, Q
						Hδ	6358	9 ± 0.67	2587 ± 692	3 ± 1				
						Hγ	6730	37 ± 3.6	4230 ± 500	26± 3				
						Hβ	7526	50 ± 6	3042 ± 285	47 ± 5				
						[OIII]	7749	11 ± 2	482 ± 181	14 ± 1				
7	09 45 56.68	−21 16 53.61	1,**2**	1200	+63	CIV	3770.8	2.57 ± 0.29	900 ± 500	-	1.437	0.002		S, Q
						HeII	3999	0.21 ± 0.14	-	31 ± 12				
						CIII]	4658	0.49 ± 0.06	1000 ± 600	22 ± 5				
8	09 57 30.06	−21 30 58.90	**1**		-	[OII]	4737	-	500 ± 300	56 ± 19	0.271	0.001		S
9	09 49 35.46	−21 56 23.30	**1**		-	-	-	-	-	-	0.242	0.002		S
10	09 47 26.99	−21 26 33.40	**1**		-	MgII	-	-	-	-	1.074**s**	-		S, Q
11	09 53 29.55	−20 02 12.6	**2**	1200	+0	CIV	4012.6	5.00 ± 0.61	4320 ± 1330	63 ± 10	1.589	0.001		S, Q
						CIII]	4941	0.77 ± 0.10	1280 ± 428	15 ± 2				
12	09 46 41.12	−20 29 26.70	**1**		-	[NeV]	6235.6	-	-	10 ± 3	0.821	0.0005		S
						[OII]	6787.4	-	587 ± 213	31 ± 6				
13	09 54 28.99	−21 56 54.93	1,**4**	2400	+90	Lyα	4802.0	5.47 ± 0.55	1360 ± 280.	-	2.950	0.001		S, N
						CIV	6117.5	0.87 ± 0.10	1310 ± 413	-				
14	09 54 47.64	−20 59 44.15	1,2	3600	+25	-	-	-	-	-	-	-	1.45	K
15	09 46 50.99	−20 53 18.23	1,**3**	5400	+90	-	-	-	-	-	-	-	1.42	K
16	09 57 51.42	−21 33 22.65	1,**2**	3600	+139	Lyα	5017	0.18 ± 0.02	-	-	3.126**s**	-		S, N

Table A1: Results of spectroscopy observing for CENSORS. Sources are labelled in terms of their CENSORS number (note that for archival purposes readers should refer to Paper I for the appropriate EISD reference). All run 1 observations were 5400s so to avoid overcrowding the table these are not included in column 5. Instead column 5 includes the exposure times for any other observations, in the order in which they are listed in column 4. Positions are the positions targetted which may be from the I–band, K–band or in some cases the position of an unresolved radio core (Papers 1 and 2). A **?** following the redshift indicates that the assigned redshift is uncertain (see notes on particular objects). An '**s**' indicates a reasonably good single line redshift and an '**s?**' indicates a single line redshift with less certainty. In the last column an 'N' indicates that there is a note on this target in the text; an 'S', 'I', 'K' or 'KL' indicates the redshift is based upon spectroscopic measurements, an I or K–band magnitude, or limit, respectively; an 'SB' or a 'Q' indicates that the source was identified as a starburst or quasar in Section 5.1.

CEN	RA	DEC	Run	Exp. Time (s)	Slit PA	Line	$\Lambda_{\rm obs}$ Å	$10^{-16}\times$ Flux erg/s/cm^2	$\Delta v_{\rm FWHM}$ kms^{-1}	W	z	Δz	z_K	Note
17	09 52 43.02	−19 58 21.60	**1**		-	[OII]	7055	-	-	-	0.893**s**	-		S, N
18	09 55 13.58	−21 23 02.40	**1**		-	Hα	7281	-	2208 ± 80	54 ± 5	0.109	0.001		S, N
						Hβ	5395	-	3110 ± 369	31 ± 3				
						[OIII]	5548	-	409 ± 38	9 ± 1				
19	09 53 30.53	−21 36 02.82	1,4	3600	+2	-	-	-	-	-		-	1.21	K
20	09 46 04.55	−21 15 04.80	1,**2**	3600	+159	HeII	3897	0.63 ± 0.13	-	-	1.377	0.001		S, N
						CIII]	4539	0.52 ± 0.07	-	-				
21	09 47 58.95	−21 21 50.50	1,2	3600	+0	-	-	-	-	-		-	1.22	K
22	09 57 30.83	−21 32 39.13	1,2	3600	+0	-	-	-	-	-		-	0.91	K
23	09 56 30.05	−20 01 26.89	1,2	3600	+10	-	-	-	-	-		-	1.93	K
24	09 54 38.33	−21 04 25.10	1,**2**	1780	+0	Lyα	5392	0.70 ± 0.07	557 ± 262	-	3.431	0.004		S
						CIV	6861	0.23 ± 0.02	391 ± 391	-				
25	09 48 04.05	−21 47 36.80	1,2	3600	+0	-	-	-	-	-		-	2.02	K
26	09 52 17.69	−20 08 36.20	1,2	3600	+0	-	-	-	-	-		-	$\geq$1.04	KL
27	09 51 49.83	−21 24 57.46	**3**	1800	+90	[NeV]	4872	1.55 ± -.2	1257 ± 520	8 ± 2	0.423	0.001		S
						[OII]	5303	0.54 ± 0.18	-	8 ± 1				
						[OIII]	7102	9.73 ± 0.9	-	28 ± 3				
						[OIII]	7125	5.07 ± 0.6	549 ± 185	19 ± 2				
28	09 46 32.15	−20 26 15.50	1,**5**	1800	-	[OII]	5486	1.2 ± 0.1	-	7 ± 1	0.471	0.001		S
						[OIII]	7360	1.54 ± 0.2	554 ± 270	5± 1				
29	09 48 15.73	−21 40 06.00	**1**		-	MgII	5497	-	5231 ± 309	46 ± 5	0.965	0.001		S, Q
30	09 54 56.01	−20 28 32.80	**1**		-	-	-	-	-	-	0.108	0.001		S
31	09 45 19.79	−21 42 38.16	3	5400	-	-	-	-	-	-		-	$\geq$ 0.88	KL, N
32	09 51 40.85	−20 11 16.33	1,**2**	2400	+0	[OII]	8015	0.43 ± 0.06	387 ± 246	-	1.151**s**	-		S, N
33	09 53 05.00	−20 44 13.88	1,**2**	3600	+142	[OII]	8211	0.13 ± 0.06	-	4 ± 2	1.203**s**	-		S, N
34	09 47 53.61	−21 47 19.30	1,8	3600	+46.6	-	-	-	-	-		-	1.32	K, N
35	09 54 52.45	−21 19 28.60	**1**		-	-	-	-	-	-	0.473	0.0004		S,
36	09 49 33.24	−21 27 07.68	1,2, **8**	3600, 4800	+34.2	[OII]	9260	0.25 ± 0.04	628 ± 300	26 ± 6	1.485**s**	0.001		S, N
37	09 49 19.53	−21 51 33.78	1,**4**	2400	+90	MgII	4225	0.80 ± 0.10	4156 ± 1213	147 ± 25	0.511	0.001		S, Q
						[NeV]	5189	0.73 ± 0.09	7788 ± 5079	244 ± 63				

Table A1: *continued.*

Source	RA	DEC	Runs	Exp. Time (s)	Slit PA	Line	Λ_{obs} Å	$10^{-16}\times$ Flux erg/s/cm^2	Δv_{FWHM} kms^{-1}	EW	z	Δz	z_K	Note
38	09 51 16.91	−20 56 37.21	1,**2**	2400	+56	Lyα	3784	256 ± 29.8	4752 ± 387	56 ± 6	2.116	0.004		S, Q, N
						SiIV+OIV	4354	12.7 ± 1.27	4194 ± 1098	4 ± 0.				
						CIV	4825	49.5 ± 5.45	4222 ± 302	22 ± 2				
						HeII	5118	2.40 ± 0.41	692 ± 284	2 ± 0.				
						CIII]	5946	21.4 ± 2.45	3636 ±321	16 ± 2				
39	09 48 36.08	−21 06 22.43	1,**3**	3600	+54	CIV	3976	9.32 ± 1.2	7467 ± 1659	63 ± 7	1.572	0.003		S, Q
						HeII	4227	0.11 ± 0.2	-	9 ± 1				
						CIII]	4902	1.13 ± 0.2	4890 ± 3662	10 ± 2				
40	09 50 59.01	−21 14 24.36	3, **8**	5400, 2400	+134,+131	[OII]	8041	1.06 ± 0.11	862 ± 178	41 ± 5	1.158	0.001		S
41	09 49 18.16	−20 54 44.70	**1**		-	-	-	-	-	-	0.295	0.001		S
42	09 52 01.59	−21 15 53.02	1,**4**	2400	+67	CIII]	4303	0.14 ± 0.02	-	21 ± 4	1.254**s?**	0.002		S, N
43	09 52 59.15	−21 48 42.46	1,**3**	5400	+145	[OII]	6629	0.53 ± 0.09	502 ± 303	18 ± 3	0.778	0.001		S
44	09 54 27.08	−20 29 46.50	**1**		-	MgII	5016	-	7033 ± 884	94 ± 10	0.790	0.002		S, Q
						[NeV]	6137	-	2437 ± 600	20 ± 2				
45	09 57 42.91	−20 06 36.87	1,**3**	5400	+152	-	-	-	-	-	0.796	0.001		S
46	09 54 03.05	−20 25 13.10	1,**3**	3600	+90	-	-	-	-	-	0.718	0.001		S
47	09 47 03.25	−20 50 00.80	**1**		-	-	-	-	-	-	0.508	0.0001		S
48	09 54 28.32	−20 39 26.90	**8**	1382	+79.4	CIV	4038	5.64 ± 0.57	4372 ± 450	35 ± 4	1.606	0.003		S, Q
						CIII]	4943	2.85 ± 0.29	8740 ± 1688	27 ± 3				
						MgII	7291	1.03 ± 0.11	3822 ± 900	16 ± 2				

Table A1: *continued.*

CEN	RA	DEC	Run	Exp. Time (s)	Slit PA	Line	Λ_{obs} Å	$10^{-16}\times$ Flux erg/s/cm^2	Δv_{FWHM} kms^{-1}	W	z	Δz	z_K	Note
49	09 53 23.21	−20 13 43.50	**1**		-	[OII]	5253	-	352 ± 197	16 ± 2	0.410	0.001		S, N
						[NeIII]	5453	-	424 ± 202	13 ± 2				
						Hδ	5784	-	1730 ± 1031	8 ± 2				
						Hγ	6141	-	4223 ± 751	72 ± 8				
						Hβ	6850	-	577 ± 165	31 ± 3				
						[OIII]	6989	-	348 ± 145	33 ± 4				
						[OIII]	7057	-	468 ± 140	114 ± 12				
50	09 52 12.70	−21 02 36.65	1,**2**	3600	+105	CIII]	4826	0.22 ± 0.05	1118 ± 900	-	1.528**?**	-		S, N
						CII]	5883	0.27 ± 0.04	335 ± 311	-				
51	09 51 23.23	−21 51 53.35	1,**4**	1200	+0	-	-	-	-	-		-	2.96	K
52	09 45 42.61	−21 15 43.59	1,**2**	1200	+0	CIV	4069	1.34 ± 0.25	3299 ± 2338	70 ± 26	1.6245	0.002		S, N
						CIII]	5004	1.00 ± 0.15	3494 ± 1732	182 ± 91				
						CII]	6106	0.23 ± 0.07	1704 ± 1663	-				
53	09 51 32.39	−21 00 28.90	**1**		-	-	-	-	-	-	0.426	0.001		S
54	09 53 20.59	−21 43 58.80	**1**		-	-	-	-	-	-	0.410	0.001		S
55	09 49 30.81	−20 23 34.71	1,**3**	3600	+78	-	-	-	-	-	0.557	0.01		S, N
56	09 50 43.16	−21 26 41.29	1,3,**8**	5400, 3600	+10,+8	[OI]	9254	0.25 ± 0.03	275 ± 144	60 ± 9	1.483**s?**	0.001		S, N
57	09 51 21.03	−21 29 54.79	1,4,8	2400,2400	+115,+23	-	-	-	-	-		-	1.20	K
58	Excluded from the sample													
59	09 48 42.52	−21 52 24.84	1,3,**8**	2400	+20, +22.5	-	-	-	-	-	1.071	0.001		S
60	09 51 48.67	−20 31 52.38	1,2	3600	+0	-	-	-	-	-		-	1.62	K
61	09 48 01.98	−20 09 11.84	1,2	3600	+114	-	-	-	-	-		-	1.45	K
62	09 49 45.86	−21 50 06.47	1,**3**	3600	+90	-	-	-	-	-	0.574	0.001		S
63	09 45 29.53	−21 18 51.60	**1,6**	900	-	-	-	-	-	-	0.314**?**	-		S, N
64	-		1		-	-	-	-	-	-		-	≥0.75	KL
65	09 57 25.98	−20 13 04.03	1,**3**	3600	+0	-	-	-	-	-	0.549	0.001		S, N

Table A1: *continued.*

CEN	RA	DEC	Run	Exp. Time (s)	Slit PA	Line	$\Lambda_{\rm obs}$ Å	$10^{-16}\times$ Flux erg/s/cm^2	$\Delta v_{\rm FWHM}$ kms^{-1}	W	z	Δz	z_K	Note
66	09 50 46.42	−21 32 55.72	1,**3**	1800	+90	[OII]	5050	2.16 ± 0.33	1305 ± 503	80 ± 17	0.355	0.001		S
						[OIII]	6780	0.74 ± 0.14	-	16 ± 4				
67	09 57 31.77	−21 20 29.24	1,**3**	1800	+90	-	-	-	-	-	0.428	0.001		S
68	09 54 51.97	−21 30 16.59	1,**3**	3600	+90	[OII]	5628	0.53 ± 0.12	-	10 ± 2	0.514	0.001		S
69	09 56 02.45	−21 56 03.80	1		-	-	-	-	-	-		-	≥ 0.59	KL
70	09 48 10.61	−20 00 58.60	1,**8**	1690	+48.6	[OII]	6134	-	-	-	0.645	0.031		S, N
						[OIII]	8237	-	-	-				
71	09 55 41.88	−20 39 38.17	1,**7**	1800	+99.7	Lyα	4691	0.01 ± 0.09	1936 ± 434	153 ± 56	2.857**s**	0.002		S, N
72	09 45 42.61	−21 15 43.59	1,**3**	2400	+0	Lyα	4167	0.46 ± 0.04	2593 ± 468	41 ± 7	2.427**s**	0.002		S, N
73	09 56 28.09	−20 48 44.95	1,2	3600	+152	-	-	-	-	-		-	1.36	K
74	09 49 30.11	−21 29 39.90	1,**8**	2400	-27	[OII]	6212	0.51 ± 0.05	-	21 ± 2	0.667	0.001		S
						Hβ	8100	-	-	-				
						[OIII]	8344	-	-	-				
75	09 45 26.92	−20 33 52.80	**1**		-	-	-	-	-	-	0.265	0.001		S
76	09 57 46.06	−21 23 27.70	**15**	600	-	-	-	-	-	-	0.282	0.001		S
77	09 49 42.95	−20 37 45.17	1,**4**	2400	+90	HeII	4120	0.15 ± 0.02	-	42 ± 18	1.512	0.0003		S
						CIII]	4795	0.09 ± 0.02	1384 ± 1127	30 ± 12				
78	09 55 59.27	−20 42 52.80	1, **8**	1507	+90	-	-	-	-	-	0.413	0.001		S
79	09 45 48.50	−21 59 06.10	1,**2**	3600	+0	[OII]	8406	0.82 ± 0.09	1115 ± 322	41 ± 7	1.255**s?**	-		S
80	09 54 53.20	−21 15 12.90	**1**		-	-	-	-	-	-	0.366	0.0001		S
81	09 54 16.45	−21 29 04.26	1,**3**	1800	+153	[OII]	5448	2.1 ± 0.2	-	36 ± 5	0.462	0.002		S
						[OIII]	7315	1.8 ± 0.2	-	35 ± 5				
82	09 50 53.08	−21 33 03.90	1		-	-	-	-	-			-	≥ 0.54	KL, N
83	09 51 29.71	−20 16 42.78	1,**3**	1800	+90	[OII]	5669	2.31 ± 0.29	926 ± 281	49 ± 6	0.521	0.0004		S
						[OIII]	7536	2.72 ± 0.31	1117 ± 266	31 ± 4				
						[OIII]	7615	1.10 ± 0.15	-	13 ± 2				
84	09 55 43.52	−21 25 27.10	1,7	4404	+90	-	-	-	-	-		-	1.92	K
85			-	-	-	-	-	-	-	-		-	≥ 1.20	KL
86	09 48 04.25	−20 34 35.00	4	2400	+126	-	-	-	-	-		-	0.82	K
87			-	-	-	-	-	-	-	-		-	≥ 1.26	KL
88	09 45 20.95	−22 01 21.00	**2**	3600	+0	[OII]	7691	0.26 ± 0.04	-	-	1.064**s?**	-		S, N
89	09 53 09.44	−20 01 20.61	**4**	2400	+64	[OII]	7118	0.17 ± 0.02		22 ± 3	0.909	0.0004		S, N
90	09 47 34.47	−21 26 58.00	1		-	-	-	-	-	-		-	≥ 1.26	KL
91	09 48 22.19	−21 05 08.43	3	5400	+52	-	-	-	-	-		-	1.24	K

Table A1: *continued.*

CEN	RA	DEC	Run	Exp. Time (s)	Slit PA	Line	$\Lambda_{\rm obs}$ Å	$10^{-16}\times$ Flux erg/s/cm^2	$\Delta v_{\rm FWHM}$ kms^{-1}	W	z	Δz	z_K	Note
92	09 52 55.92	−20 51 44.90	**1**		-	MgII	4943	-	$\sim$ 4300	-	0.743	0.001		S
						[NeV]	5980	-	-	-				
						[OII]	6496	-	-	-				
						[OIII]	6740	-	-	-				
93	09 46 19.14	−20 37 57.60	**1**		-	-	-	-	-	-	0.183	0.0005		S
94	09 45 21.12	−20 43 21.40	1,2	3600	+122	-	-	-	-	-		-	1.65	K
95	09 54 21.48	−21 48 07.20	**1**		-	Hα	6857	-	263 ± 144	42 ± 4	0.045	0.001		S
					-	[SII]	7023	-	859 ± 196	7 ± 1				
96	09 49 25.99	−20 05 20.20	1,**2**	2400	+0	Lyα	4506	0.44 ± 0.07	-	-	2.706**s?**	-		S
97			-	-	-	-	-	-	-	-		-	1.64	K
98	09 49 35.18	−21 58 10.45	1,4	3600	+90	-	-	-	-	-		-	1.64	K
99	09 57 02.29	−21 56 51.23	1,**3**	3600	+90	-	-	-	-	-	0.738	0.0006		S
100	09 50 48.54	−21 54 56.71	1,3	1800	+73	-	-	-	-	-		-	1.29	K
101	09 52 50.42	−21 31 47.6	1,4,**8**	5400, 3600	+90, +115.4	-	-	-	-	-	1.043**?**	-		S, N
102	09 46 49.47	−21 16 46.40	**3**	1800	+40	-	-	-	-	-	0.468	0.0004		S, N
103	09 47 30.81	−21 28 29.10	1		-	-	-	-	-	-		-	$\geq$ 1.26	KL
104	09 57 39.07	−20 03 20.19	1,2	3600	+12	-	-	-	-	-		-	0.88	K
105	09 47 24.38	−21 05 02.30	1,**4**	3600	+90	Lyα	5322	0.50 ± 0.05	864 ± 283	-	3.377**s**	-		S, N
106	09 56 07.00	−20 05 44.3	1,3,8	1800, 4800	+140, +131.3	-	-	-	-	-		-	1.29	K
107	09 45 38.08	−21 11 13.50	1,**3**	3600	+90	-	-	-	-	-	0.512	0.001		S
108	09 56 49.78	−20 35 25.80	**1**		-	[OII]	4587	-	694 ± 332	9 ± 2	0.230	0.001		S
109	09 52 10.91	−20 50 09.30	1,3,4	5400, 3600	+0,+0	-	-	-	-	-	-		0.72	K
110	09 55 11.46	−20 30 19.24	**3**	1800	+90	-	-	-	-	-	0.282	0.0002		S
111	09 47 44.75	−21 12 23.30	**1**		-	-	-	-	-	-	0.411	0.01		S
112	09 56 42.30	−21 19 44.30	1,3,7	5400, 3600	+51, +121	-	-	-	-	-		-	1.75	I
113	09 47 10.31	−20 35 52.40	1,3	5400	+90	-	-	-	-	-		-	0.94	K
114	09 56 04.45	−21 44 36.59	1,**3**	1800	+90	HeII	3972	0.70 0.18	-	12 5	1.426	0.004		S, Q, N
						CIII]	4626	2.71 0.38	3174 1262	60 13				
						MgII	6799	5.75 0.63	5196 1608	116 17				
115	09 57 24.89	−20 22 42.90	**1**		-	-	-	-	-	-	0.545			S

Table A1: *continued.*

CEN	RA	DEC	Run	Exp. Time (s)	Slit PA	Line	Λ_{obs} Å	$10^{-16}\times$ Flux erg/s/cm^2	Δv_{FWHM} kms^{-1}	W	z	Δz	z_K	Note
116	09 57 35.36	−20 29 35.38	1,**3**	1800	+90	Lyα+NV	4468	29.2 ± 2.1	1.28E4 ± 1787	47 ± 5	2.637	0.001		S, N
						SiIV+OIV	5090	2.9 ± 0.4	3911 ± 1454	7 ± 1				
						CIV	5632	2.6 ± 0.2	1490 ± 366	4 ± 1				
117	09 54 10.51	−21 58 01.48	1,**2**	3600	+69	CIII]	4203	0.26 ± 0.06	-	-	1.204	0.002		S
						[OII]	8217	0.44 ± 0.08	1170 ± 711	-				
118	09 47 48.46	−20 48 35.22	1,**4**	5400	+157	Lyα	4006	0.23 ± 0.03	524 ± 480	48 ± 21	2.294**s?**	-		S, N
119	09 49 02.26	−21 15 04.97	1,4,**8**	5400, 3600	+90, +99.8	[OII]	9258	0.12 ± 0.04	-	-	1.484**s?**	0.002		S, N
120	09 53 57.43	−20 36 51.05	1,**3**	1800	+90	Lyα	4658	7.9 ± 0.8	3357 ± 449	75 ± 10	2.829	0.002		S
						HeII	6279	1.2 ± 0.1	840 ± 287	10 ± 2				
121	09 52 01.21	−20 24 36.10	**1**		-	[OII]	4643	-	749 ± 221	59 ± 7	0.246	0.001		S
122	09 56 37.09	−20 19 09.80	**1**		-	-	-	-	-	-	0.250	0.001		S
123	09 54 31.06	−20 35 37.66	1,3	3600	+90	-	-	-	-	-		-	0.83	K
124	09 49 10.80	−20 21 53.00	NED	-	-	-	-	-	-	-	0.01559	0.00003		S, N
125	09 49 22.34	−21 18 17.70	**1**		-	[NeV]	5825	-	-	-	0.701	0.001		S
126	09 47 50.32	−21 42 10.10	1		-	-	-	-	-	-		-	0.38	K, N
127	09 49 24.62	−21 11 11.61	1,**3**	3600	+90	[OII]	7163	1.8 ± 0.2	669 ± 215	21 ± 3	0.922**s**	-		S, N
128	09 49 02.78	−20 16 10.90	1		-	-	-	-	-	-		-	1.12	K
129	09 52 26.41	−20 01 07.09	1,**2**	1200	+85	Lyα	4161	1.7 ± 0.2	2064 ± 254	-	2.421	0.003		S, N
						CIV	5303	0.69 ± 0.08	1403 ± 196	64 ± 28				
						CIII]	6524	0.40 ± 0.06	902 ± 196	-				
130	09 57 22.17	−21 01 05.34	1,4	3600	+90	-	-	-	-	-		-	2.88	K

Table A1: *continued.*

CEN	RA DEC	Run	Exp. Time (s)	Slit PA	Line	$\Lambda_{\rm obs}$ Å	$10^{-16}\times$ Flux erg/s/cm^2	$\Delta v_{\rm FWHM}$ kms^{-1}	W	z	Δz	z_K	Note
131	09 51 49.02 −21 33 39.90	**1**		-	-	-	-	-	-	0.470	0.01		S, N
132	09 46 02.37 −21 51 44.15	4, 7	1800, 5400	+90, +107	-	-	-	-	-		-	2.55	K
133	09 51 29.42 −20 25 35.36	**8**	2400	+74.1	[OII]	8701	0.36 ± 0.10	825 ± 521	36 ± 16	1.335**s?**	0.003		S, N
					[SII]	6913	-	872 ± 167	13 ± 1				
134	09 53 44.47 −21 36 01.75	**4**	3600	+0	Lyα	4079	0.49 ± 0.05	1452 ± 494	53 ± 15	2.355	0.003		S
					CIV	5201	0.35 ± 0.04	703 ± 287	41 ± 7				
					HeII	5504	0.31 ± 0.03	-	36 ± 6				
					CIII]	6395	0.21 ± 0.02	402 ± 251	31 ± 7				
135	09 47 47.93 −21 00 45.40	1,**8**	2400	+42.5	MgII	6483	1.31 ± 0.13	6599 ± 504	26 ± 3	1.316**s?**	0.002		S, N
136	09 54 42.16 −20 49 48.93	1, **7**	1800	-35.5	[OII]	6066	0.01 ± 0.001	-	19 ± 4	0.629	0.001		S, N
					Hβ	7921	0.01 ± 0.002	-	14 ± 3				
137	09 50 38.66 −21 41 11.39	**3**	3600	+165	-	-	-	-	-	0.526	0.001		S
138	09 55 26.95 −20 46 05.90	**4**	3600	+90	[OII]	5622	0.11 ± 0.05	-	10 ± 2	0.508	0.001		S
139	09 49 12.74 −22 00 23.40	**1**		-	-	-	-	-	-	0.344	0.001		S
140	09 45 26.32 −21 55 00.10	**1**		-	-	-	-	-	-	0.265	0.002		S
141	09 45 50.99 −20 14 46.26	1,**2**	2400	+108	Lyα	4656	0.44 ± 0.07	1672 ± 910	-	2.829**s?**	-		S, N
142	09 53 44.47 −21 36 01.75	1,4	1800	+0	-	-	-	-	-		-	2.78	K
143	09 47 46.09 −21 27 50.60	1,2	3600	+160	-	-	-	-	-		-	1.88	K
144	09 49 59.71 −21 27 18.29	**4**	3600	+0	[OII]	6321	0.54 ± 0.07	878 ± 444	6 ± 1	0.696	0.00006		S
145	09 48 14.19 −19 59 56.28	1,**3**	5400	+90	-	-	-	-	-	0.40	0.02		S
146	09 50 27.69 −21 48 09.17	NED	-	-	-	-	-	-	-	0.02935	0.00003		S, N
147	09 45 21.71 −20 35 59.33	1,2	3600	+0	-	-	-	-	-		-	1.34	K
148	09 56 39.20 −20 10 43.60	1		-	-	-	-	-	-		-	0.67	K, N
149	09 52 14.35 −21 40 18.30	**1**		-	Hβ	4999	-	316 ± 199	24 ± 2	0.029	0.001		S
					[OIII]	5107	-	2084 ± 483	52 ± 5				
					[OIII]	5149	-	443 ± 192	34 ± 3				
					Hα	6749	-	253 ± 146	121 ± 12				
150		-	-	-	-	-	-	-	-		-	0.14	K

Table A1: *continued.*

APPENDIX B: NOTES ON INDIVIDUAL SOURCES

This section provides details on the interpretation of the spectroscopic observations in terms of both measured redshifts and whether sources are identified as starforming galaxies or quasars.

CENSORS 2: This is a single line redshift. The most likely candidates for a single line are the bright emission lines [OII] and Lyα which would place this source at $z = 0.91$ and $z = 4.87$ respectively. A K–band magnitude of 19.00(13) (where the error, in units of 0.01 mags, is given in brackets) in a $1''$aperture makes the lower redshift more likely. Adding further weight to that conclusion are two other galaxies within $6''$and on either side, which also have single emission lines at wavelengths within 100Å of the detected line. It is therefore likely that these three galaxies form an interacting system.

CENSORS 4: In Paper 1 two likely candidates were listed for this source. This AGN spectrum now identifies the correct host galaxy to be the northerly of those two.

CENSORS 13: This source has significantly extended Ly α emission as shown in Fig. B1.

CENSORS 16: This single line spectrum has been assigned a redshift corresponding to detection of Ly α. With a $1''$aperture K–band magnitude of 19.85 this cannot be [OII] at $z = 0.35$ according to the K–z relation. Although there is a hint of a He II (1640) confirming line in the extracted spectrum this by no means certain from the 2D image.

CENSORS 17: Identifying this line as [OII] is consistent with its 18.07(20) K–band magnitude ($1.5''$ aperture).

CENSORS 18: This object has clear broad emission lines but is identified with a low redshift, extended galaxy, and so is a broad line radio galaxy (BLRG). It is not considered a quasar in this work.

CENSORS 20: No features were found at the centre of the target. The radio structure is slightly double lobed and at the centre of the main lobe two emission lines, but no continuum, were found. These have a wavelength ratio of 1.164 which matches either CIII] and HeII or [OII] and Hβ. The latter would give a redshift of 0.04 which does not match the limiting K–band magnitude of 19.4. Hence the former line identifications are assumed.

CENSORS 31: This source has two potential host galaxy candidates based upon I and K–band imaging. However both are misaligned to the radio axis. The western candidate was identified as a star via 2df spectroscopy and the eastern candidate was then targetted with FORS1. This target is a low mass star as identified by a KI absorption feature (as compared to examples in Leggett et al. 1996). This implies that the actual host galaxy must remain undetected to a limit of 18.2 in K.

CENSORS 32: Identifying this line as [OII] is consistent with its 18.37(13) K–band magnitude ($1''$aperture).

CENSORS 33: This single line is convincing in the 2D image. The 19.17(12) K band magnitude in $1''$aperture is consistent with assigning [OII] to this line; it is not consistent with Ly α.

CENSORS 34: The spectrum has a complete absorption band at about 9200Å with width $\sim$ 100Å. This is not identified with any known spectral feature that the authors are aware of. A redshift is assigned on the basis of its K–band magnitude.

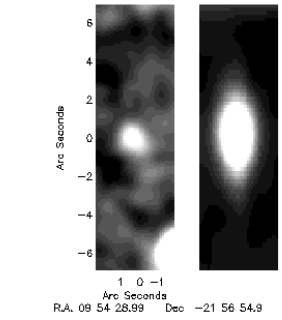

CENSORS 13

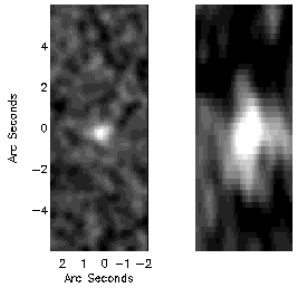

CENSORS 71

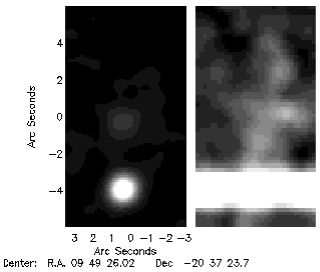

CENSORS 72

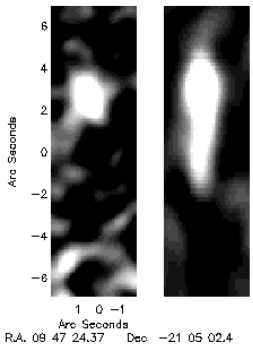

CENSORS 105

Figure B1. Extended emission in CENSORS 13, 71, 72, 105 which is believed to be Lyα emission. The left panels show the K–band image and the right hand panels show the spectrum, dispersed in the x–direction and matched spatially in the y–direction. Note that in the case of CENSORS 72 there is bright star beneath the faint host in this image, the emission associated with the host is not a feature in the stellar spectrum.

CENSORS 36: A single emission line is observed. This is assumed to be [OII] as this fits very well with the K–z relation estimate for the redshift.
CENSORS 37: Whilst this source has broad lines it is also at relatively low redshift (0.5) and is optically faint, perhaps suggesting that is better classified a BLRG. However it lies far off the K–z relation and so is classified as a quasar.
CENSORS 38: This source shows clear broad emission lines. It was not selected as a quasar on the basis of the optical image in Paper 1 because the host object was not identified there (it was below the likelihood threshold). However, it is an unresolved optical ID. It is therefore a quasar.
CENSORS 42: This single line is clear in the 2D image. With a K–band magnitude limit of 18.8 this is more likely to be Ly α or CIII] than [OII]. The K–band magnitude might suggest a mild preference for assigning Lyα as the line ID, however if that were the case there are several other lines that might be expected at higher wavelengths (e.g. CIV, HeII or CIII]) On the other hand, if the line were CIII], then the next bright line would be [NeV], which would coincide with a sky feature at 7700Å. Mg II would also be missing, but this is not always detected in every case (see CENSORS 20). Taking the line as CIII]: $z = 1.254$.
CENSORS 49: As with CENSORS 37 this may be better classified a BLRG, rather than a quasar, and as it lies consistently on the K–z relation, of Willott et al. (2003), this is the classification it is given.
CENSORS 50: There is a possible single line at 5882Å, however it is not clear from the 2D image whether this is in fact an emission line or if it is a residual associated with sky lines. There is also a faint line at 4826 Å. This is mildly visible in the 2D spectrum. To be roughly consistent with the K–band magnitude, which estimates the redshift as $z \simeq 1.6$, the 4826 Å line (which is more likely of the two to be a genuine detection) will be at rest wavelengths of $\approx$ 1850Å. The strongest line in this range is CIII] at 1909 giving $z = 1.528$. This matches the 5882 Å up to be CII] and would put HeII at 4145 Å. Whilst HeII is not clearly detected in the 2D image, there are hints of signal in the spectrum which add weight to this spectroscopic redshift.
CENSORS 52: Similarly to CENSORS 49, the line widths have large errors and the source is quite faint. As it lies in good agreement with the K–z relation of Willott et al. (2003) it is taken to be a broad line radio galaxy rather than a quasar.
CENSORS 55: This low S/N detection of the Ca H and K and the G–band absorption features is consistent with this source's K band magnitude of 17.19(09) (1″aperture).
CENSORS 56: The target was a galaxy detected in both the I and K–bands between the two radio lobes of this source. The target spectrum shows no features with which its redshift may be estimated. However the slit was aligned with the northern radio lobe and a single emission line was clearly detected there. The position of the line is shown in Figure B2 and is 09 50 43.3 −21 26 32.4 (J2000) and it is possible that this is in fact a very faint host galaxy associated with the radio source. This line is assumed to be [OII]. At such a redshift it is reasonable that no other equally strong would be seen in the spectrum. If the line were [OIII] then [OII] might also be expected.
CENSORS 63: There is a faint detection of a 4000 Å break in this spectrum from 2dF. This provides a redshift of 0.314.

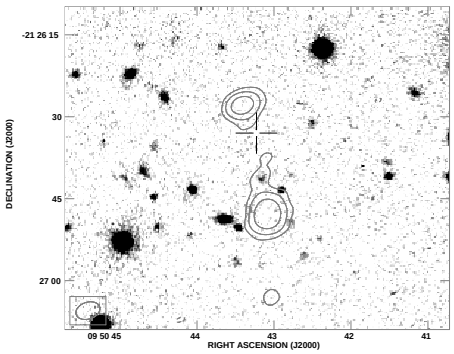

Figure B2. The greyscale presents the I–band image of CENSORS 56. The crosshairs indicate the position of the emission line detected in spectroscopic observations of the source.

This has been confirmed in the blue spectrum from ISIS on the WHT which finds a break corresponding to $z = 0.302$. Whilst this is not a strong detection, this redshift is consistent with the K–z relation estimate of 0.3. The latter redshift estimate is chosen as the 2df spectrum suffers from not being flux calibrated. This object was classified as a quasar candidate on the basis of both its stellaricity and colour in Paper 1. However its colour may not necessarily suggest that it a quasar (its B–band magnitude is very close to the survey limit). In addition no emission lines are seen in the spectrum. It is a radio galaxy.
CENSORS 65: This low S/N detections of the Ca H and K and the G-band absorption features are consistent with this source's K–band magnitude of 17.77(16) (1″aperture).
CENSORS 70: In Papers 1 and 2 the host galaxy remained unidentified from a choice of five candidates. Candidates B and E (as described in Paper 2) were considered the most likely hosts on the basis of their I–K colours. A long slit was placed on both candidates B and E. The resulting spectra showed that B was a late type star, but that E has both the [OII] and [OIII] emission lines and thus harbours an active nucleus. Candidate E, with a position of 09 48 10.6 -20 00 58.56 (J2000), is concluded to be the host galaxy.
CENSORS 71: This single line is assigned to Ly α because it is very extended in the 2D image, as shown in Fig. B1.
CENSORS 72: This single line is assigned to Ly α because it is very extended in the 2D image, as shown in Fig. B1.
CENSORS 82: The target, as identified in Paper 1 from the EIS I band imaging, is a star. A redshift lower limit is estimated on the basis of its limiting K–band magnitude.
CENSORS 88: This single line is convincing in the 2D image despite proximity to sky lines. Interestingly the target for these observations was an I–band object which was not given as the host galaxy in Paper 1 as it was below the formal likelihood limit. This object was not observed in the K–band. The I–band magnitude is 22.62 and the position is 09 45 20.95 −22 01 21.00. The line is taken to be [OII].
CENSORS 89: There were two K–band identifications for this source. The one at the centre of the extent of the radio source shows no continuum/features; the eastern identification shows the spectrum presented. The [OII] line and H and K absorption features are clear in the 2D image.
CENSORS 95: As described in Section 5.1.1 this radio source is due starformation rather than an active nucleus.
CENSORS 100: A spectrum was attempted for this source

using the ESO 3.6m telescope, however no features were observed and it was decided this was a more suitable target for the VLT. Despite the lack of features, it can be concluded that this source is not a quasar since the necessary bright emission lines would have revealed themselves in even a short exposure.

CENSORS 101: There are absorption features which appear to match H and K. However as this occurs at low S/N close to the beginning of sky residuals, it would be comforting to have confirmation. The redshift obtained from assuming these features are H and K is 1.043, which is consistent with the K–z relationship estimate of 0.985.

CENSORS 102: This galaxy is spectroscopically found at $z = 0.468$ and clearly has an old stellar population. This helps identify it as the likely host despite the lack of emission lines.

CENSORS 105: This source has very extended Ly α emission as shown in Fig. B1.

CENSORS 114: Clear broad emission lines suggest this source as a quasar. It was not classified as a quasar optically due to a S/G slightly lower than the limit, but it has a blue colour so is likely to be a quasar.

CENSORS 116: This source is interesting because of the strength of the NeV line compared to the CIV line. This rare enhancement of the NV/CIV line ratio is discussed in van Ojik et al. 1994 for the case of TX0211. According to their work, the Ly α/CIV line ratio of CENSORS 116 is typical of high redshift radio galaxies, but, taking a value of > 1.6, the NV/CIV is extremely enhanced. Following the discussion of van Ojik et al., this is likely due to enhanced nitrogen abundance or shock processes.

CENSORS 118: This single line has a very slight confirmation suggesting it could be CIII] (1909) with CII] (2326) as the extra line. However if this is the case then there is no detected [OII] 3727 emission which is unlikely, therefore it is assumed that this line is Ly α. This is also more consistent with its K–band (in a $1''$aperture) of 19.82(15) than the CIII] assignment for that line (or [OII] as a single line).

CENSORS 119: This radio source is elongated and the slit was aligned along the radio axis. No redshift was measurable on the target spectrum, however a single emission line was observed $1.4''$ to the E of the target. This is well within within the region of the radio source and it is assumed that this emission line is representative of the host redshift. Given the lack of any other emission lines, it is assumed that this is [OII], resulting in a redshift of 1.484.

CENSORS 124: This source has not been spectroscopically targetted, but a redshift of 0.01559 has been found by Mathewson et al. (1992). As described in Section 5.1.1 this radio source is due to star formation rather than an active nucleus.

CENSORS 126: There were two likely host galaxies candidates in Paper 1. Of these the western source was targetted with 2dF. This spectrum revealed that this candidate was a star. The second candidate host galaxy has not been spectroscopically targetted. It should be noted that the radio morphology for this source is unclear and it is not clear how realistic the remaining candidate is. However since the radio morphology of this source is unclear, it can be said that it is unlikely to be a quasar.

CENSORS 127: This single line is assigned to [OII] for consistency with its K–band magnitude of 17.46(21) in a $1.5''$aperture.

CENSORS 129: Ignoring the Lyα line, only the CIV permitted line is broad and this is a marginal case. Since the K–band magnitude is consistent with the K–z relation of Willott et al. (2003) is it assumed to be a radio galaxy.

CENSORS 131: There are no confirming lines or features for this 4000Å break. The K–band magnitude is 16.00(21) in a $0.6''$aperture and so a redshift of 0.470 fits with the K–z relation expectation.

CENSORS 133: A single line is detected. Assuming it to be [OII] gives a redshift of 1.335 which is consistent with the K–z relationship estimate of 1.834. If the line were [OIII] the corresponding redshift would be 1.737, however we would expect to see [OII] at the low wavelength end of the spectrum. The redshift is taken to be 1.335

CENSORS 135: A single broad line is detected along with continuum. Given the shape of the line it is assumed to be MgII, resulting in a redshift of 1.316. This is consistent with the K–z prediction however it should be noted that the continuum is blue and so this prediction is not appropriate. Since the continuum is slightly blue this source is assumed to be a quasar in order to err on the side of caution.

CENSORS 136: In Paper 2 the host galaxy for this source was identified with a faint K–band galaxy which was offset in position from the main radio lobe (to the SE). This was justified on the basis that there were indications of a mild extension in the radio structure, seen as two faint peaks south of the main lobe. The host galaxy was targetted with FORS1 with LSS with a position angle for which the slit also passed through the centre of the main radio lobe. When the spectrum was analysed, the previously identified host showed no signs of activity, however two emission lines were detected at the position of the main radio lobe. These lines are used to measure a redshift for the source of 0.629.

CENSORS 141: This single line is assigned to Ly α in agreement with the K–z relation prediction for this source ($K = 19.57(20)$ in a $1''$aperture).

CENSORS 146: This source has not been spectroscopically targetted, but a redshift of 0.02935 has been found by Mathewson & Ford (1996). As described in Section 5.1.1 this radio source is due starformation rather than an active nucleus.

CENSORS 148: The targetted object was a star and so a redshift has been estimated on the basis of its K–band magnitude.

APPENDIX C: SPECTRA OF CENSORS SOURCES

Figure C1 shows spectra of the CENSORS sources for which a spectroscopic redshift has been successfully obtained.

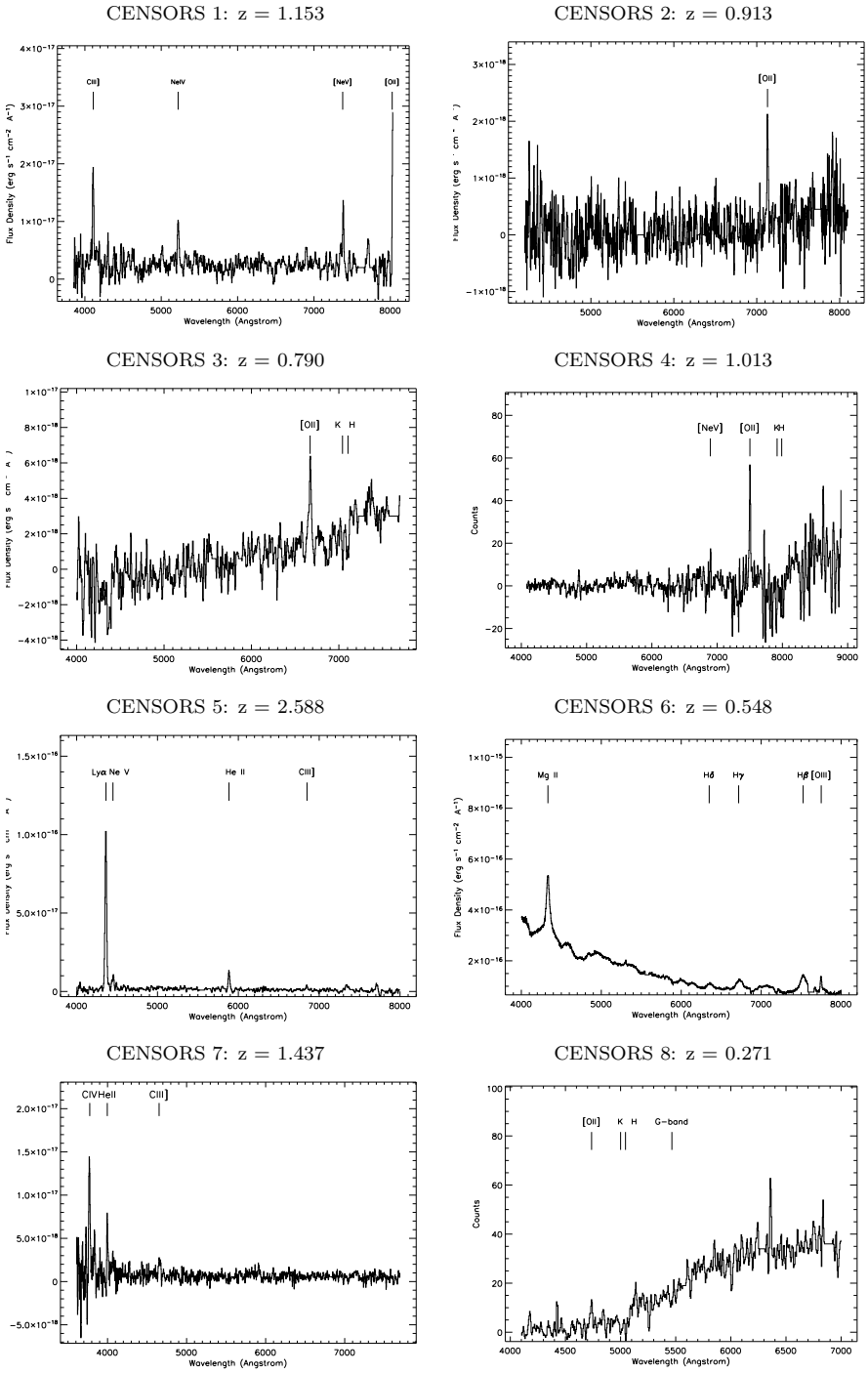

Figure C1. CENSORS spectra with redshift identifications.

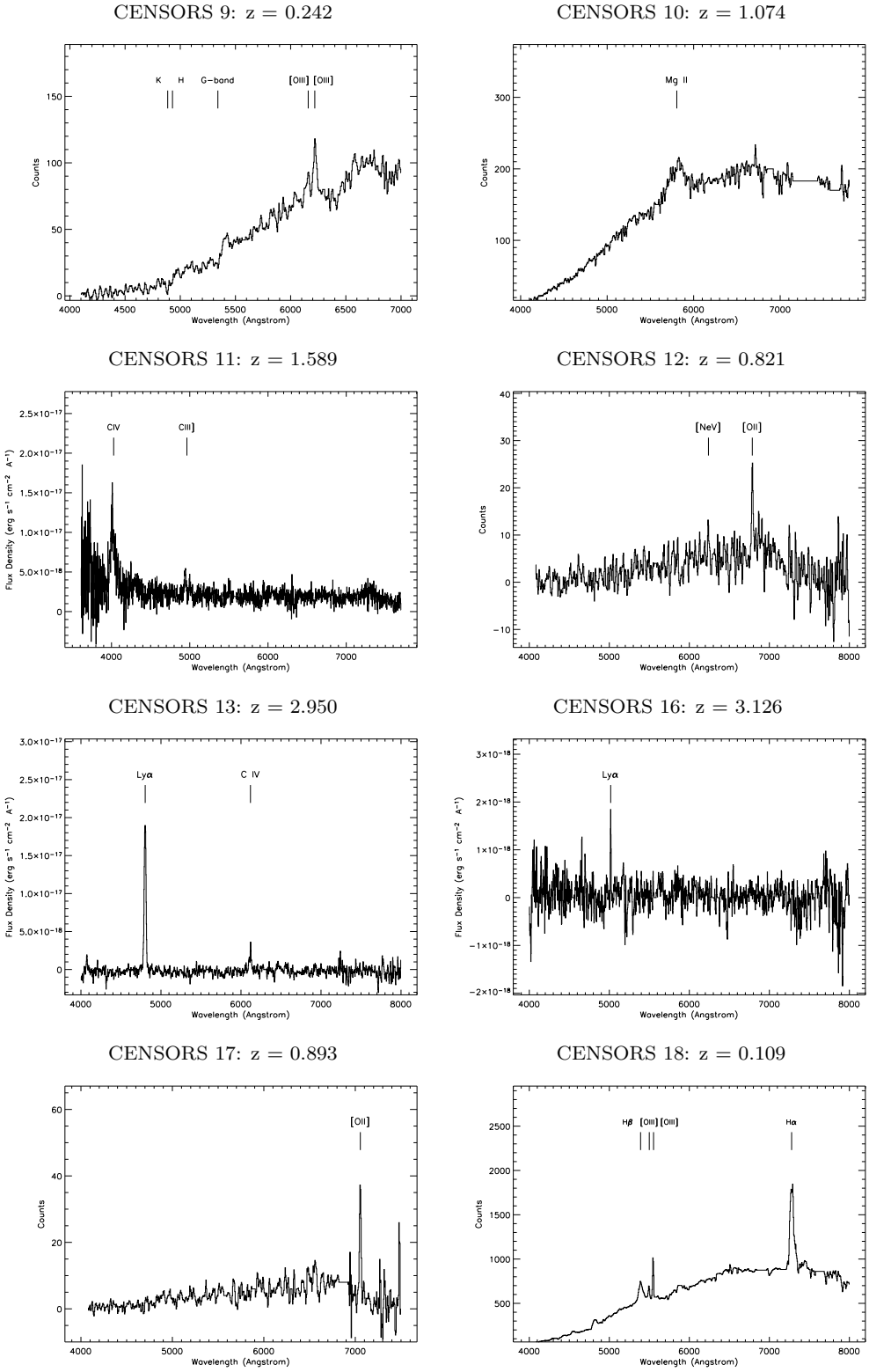

Figure C1. CENSORS spectra with redshift identifications continued.

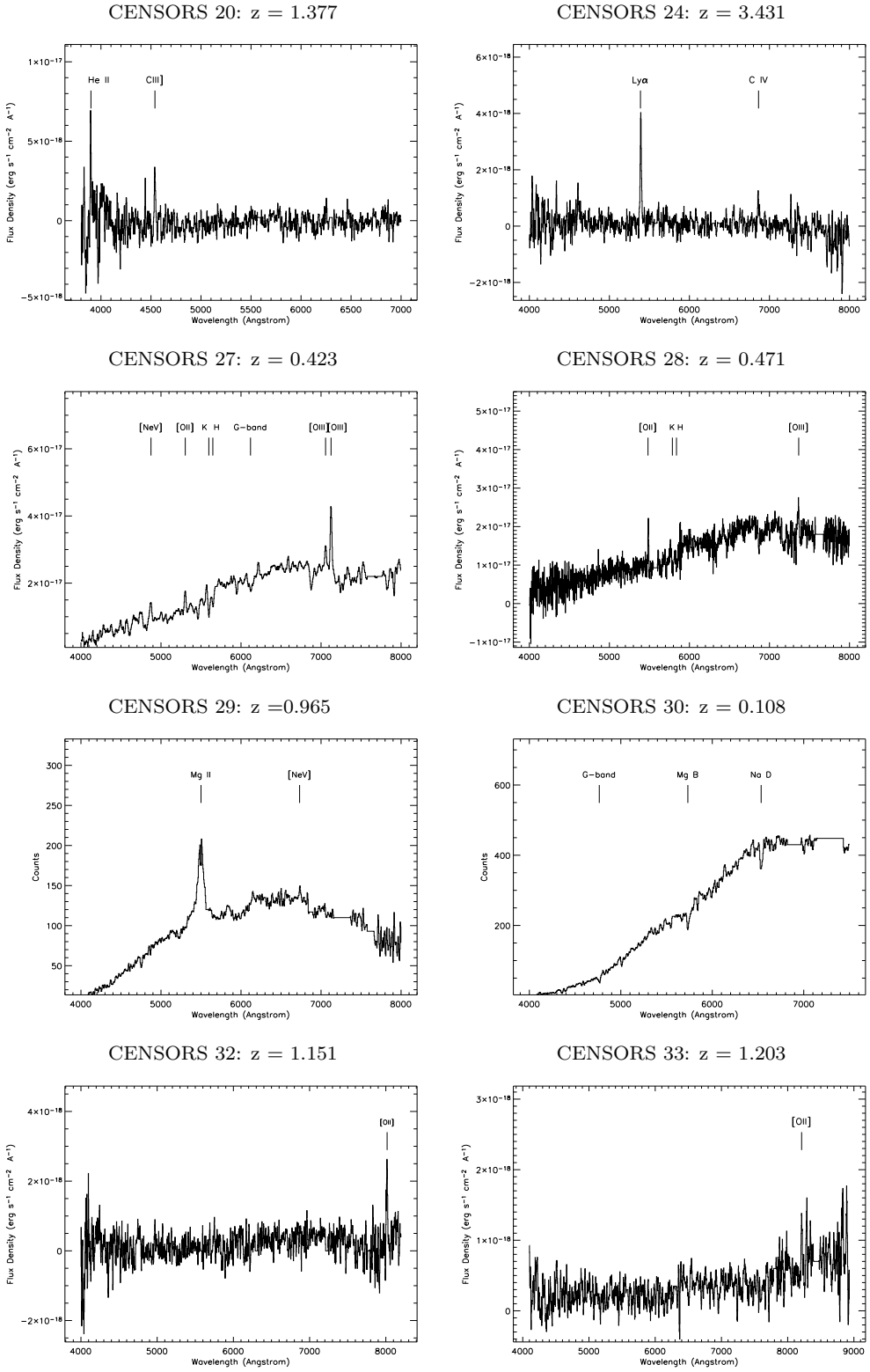

Figure C1. CENSORS spectra with redshift identifications continued.

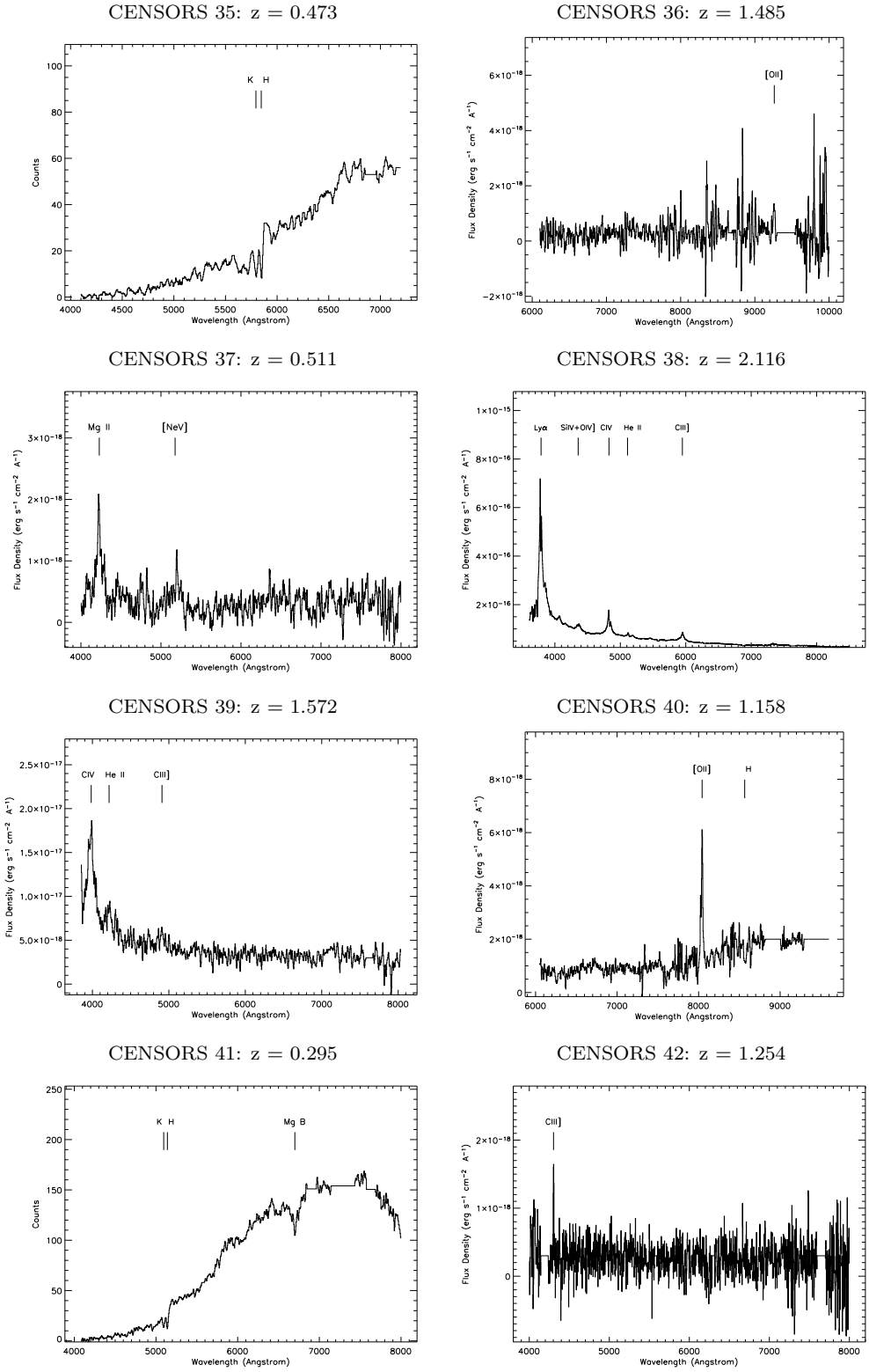

Figure C1. CENSORS spectra with redshift identifications continued.

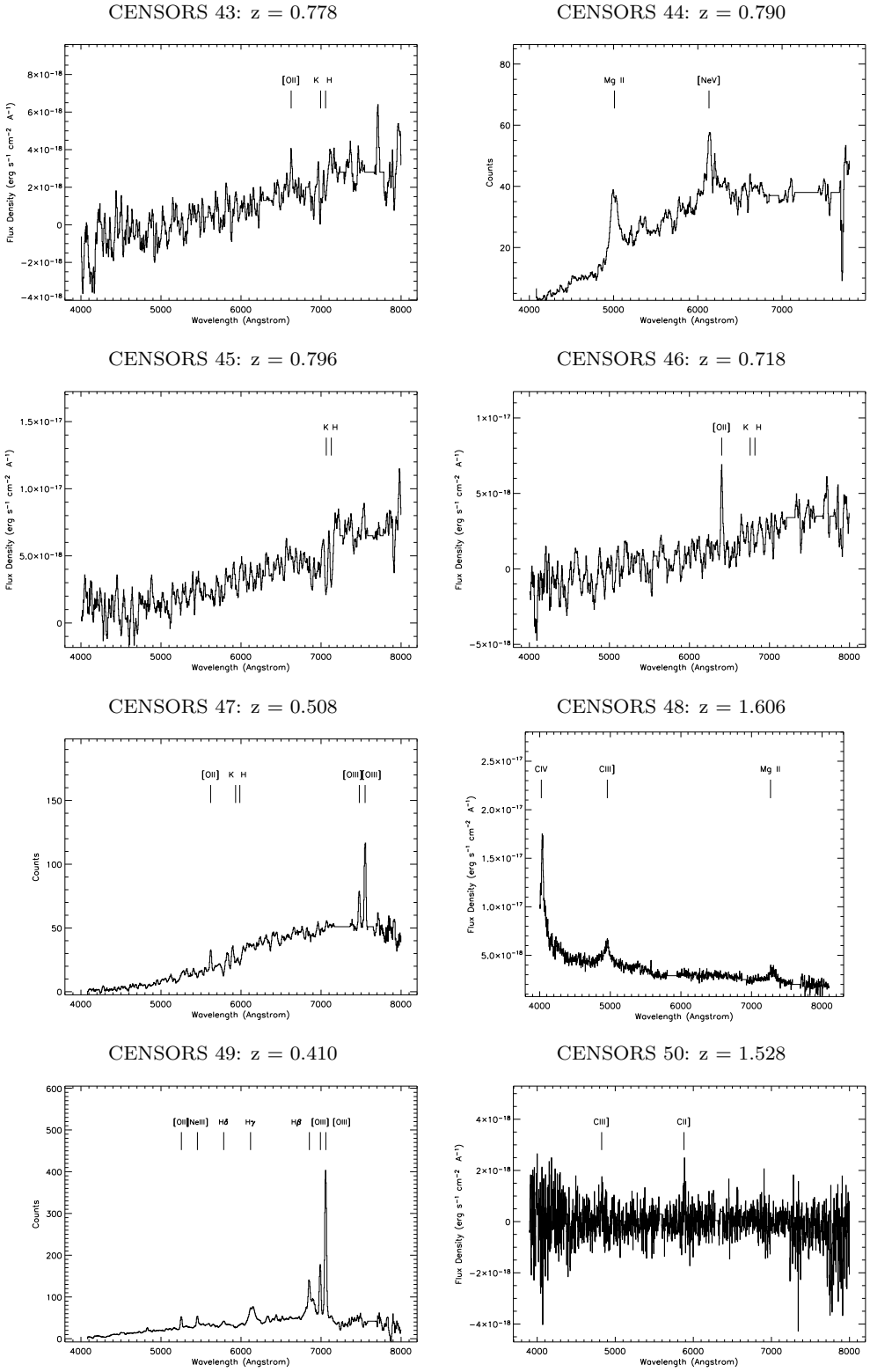

Figure C1. CENSORS spectra with redshift identifications continued.

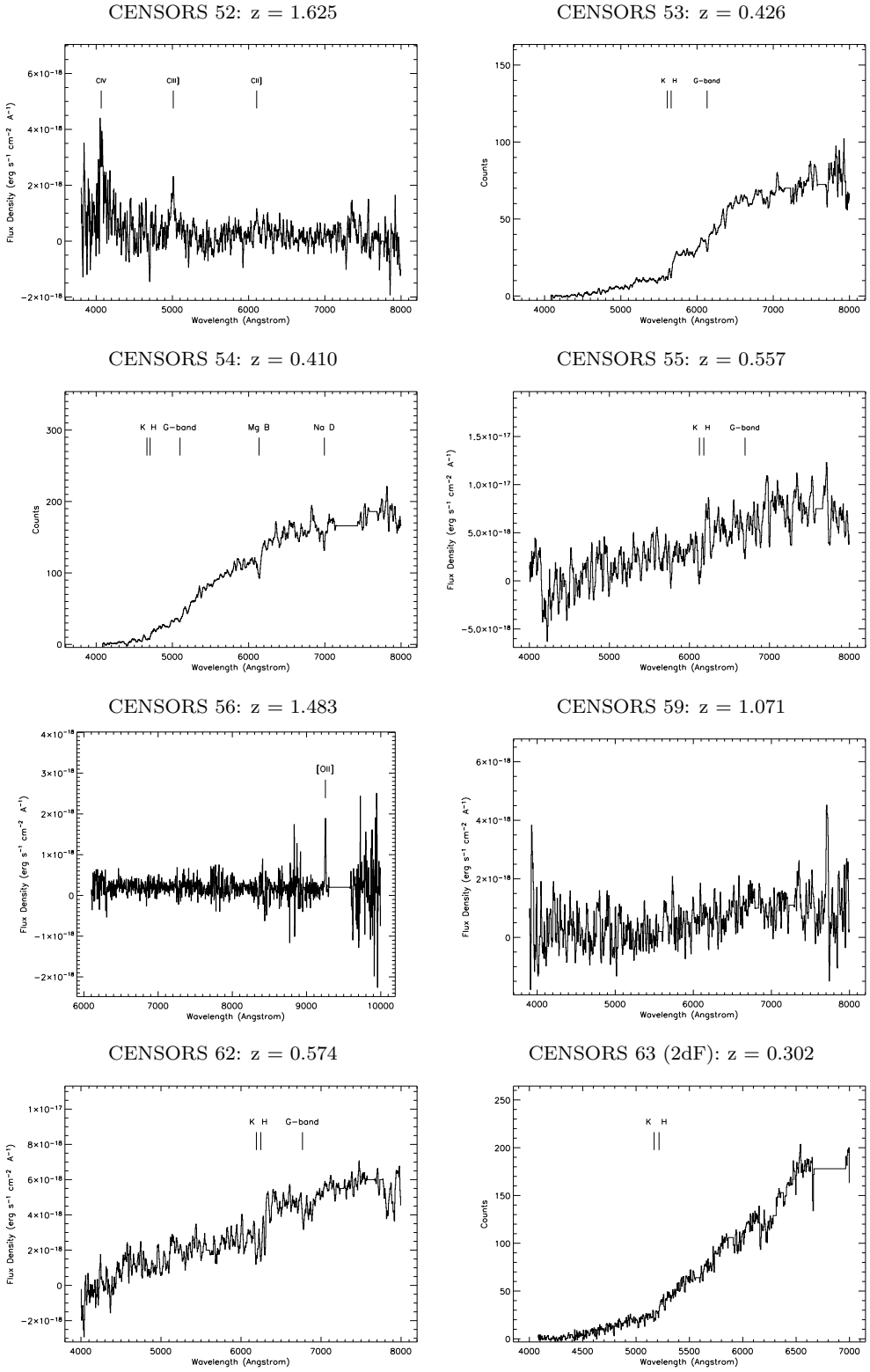

Figure C1. CENSORS spectra with redshift identifications continued.

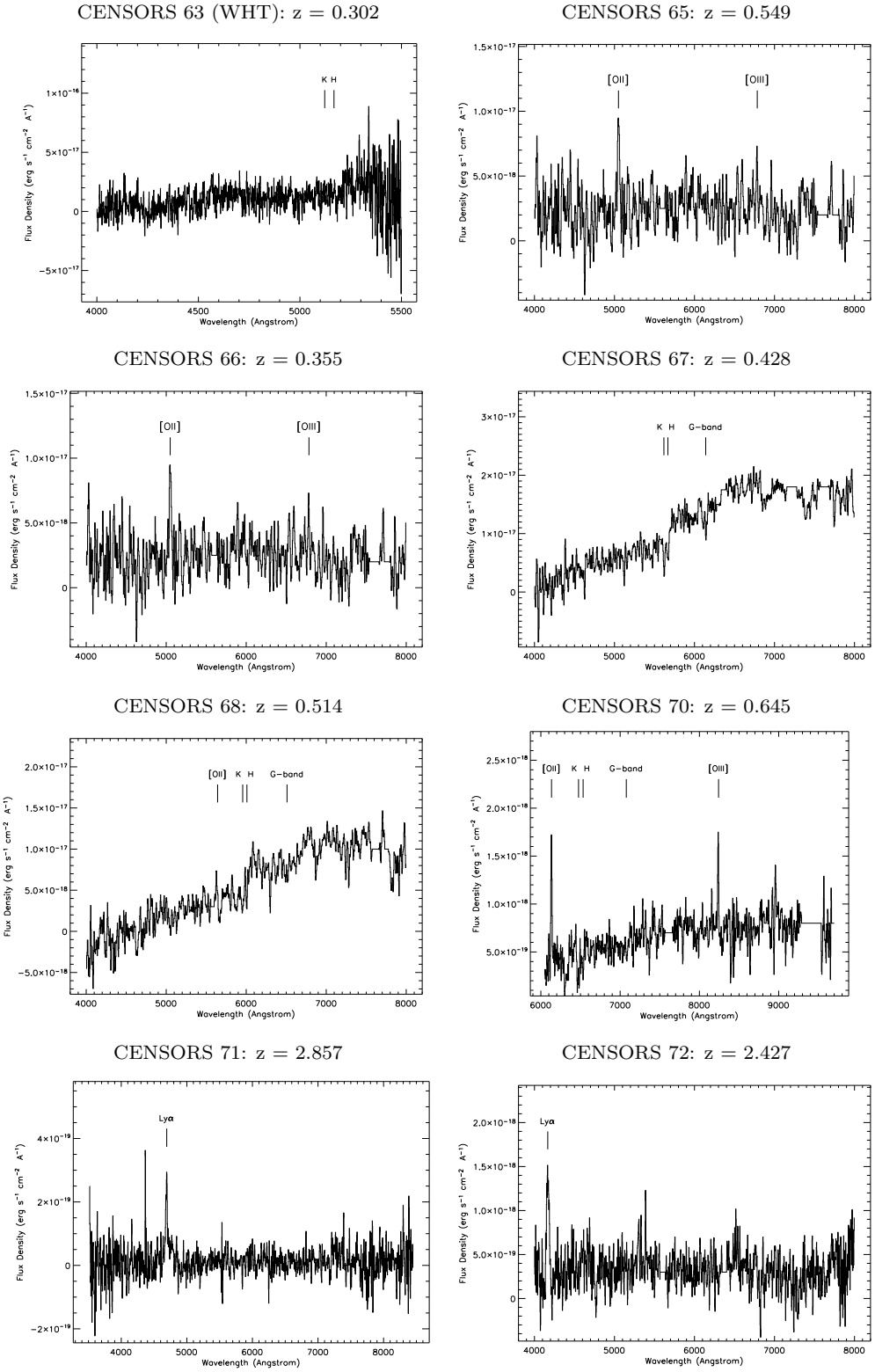

Figure C1. CENSORS spectra with redshift identifications continued.

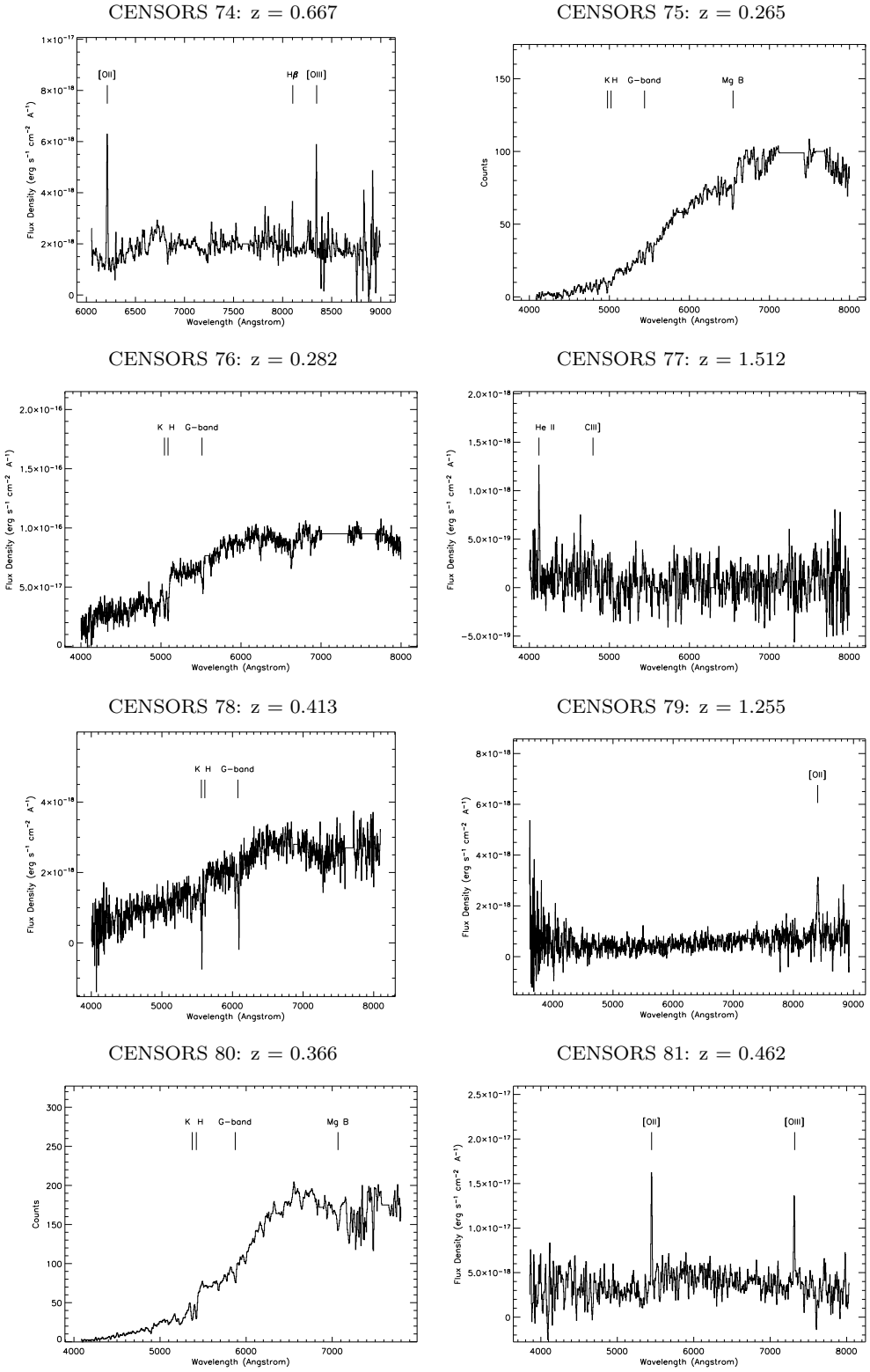

Figure C1. CENSORS spectra with redshift identifications continued.

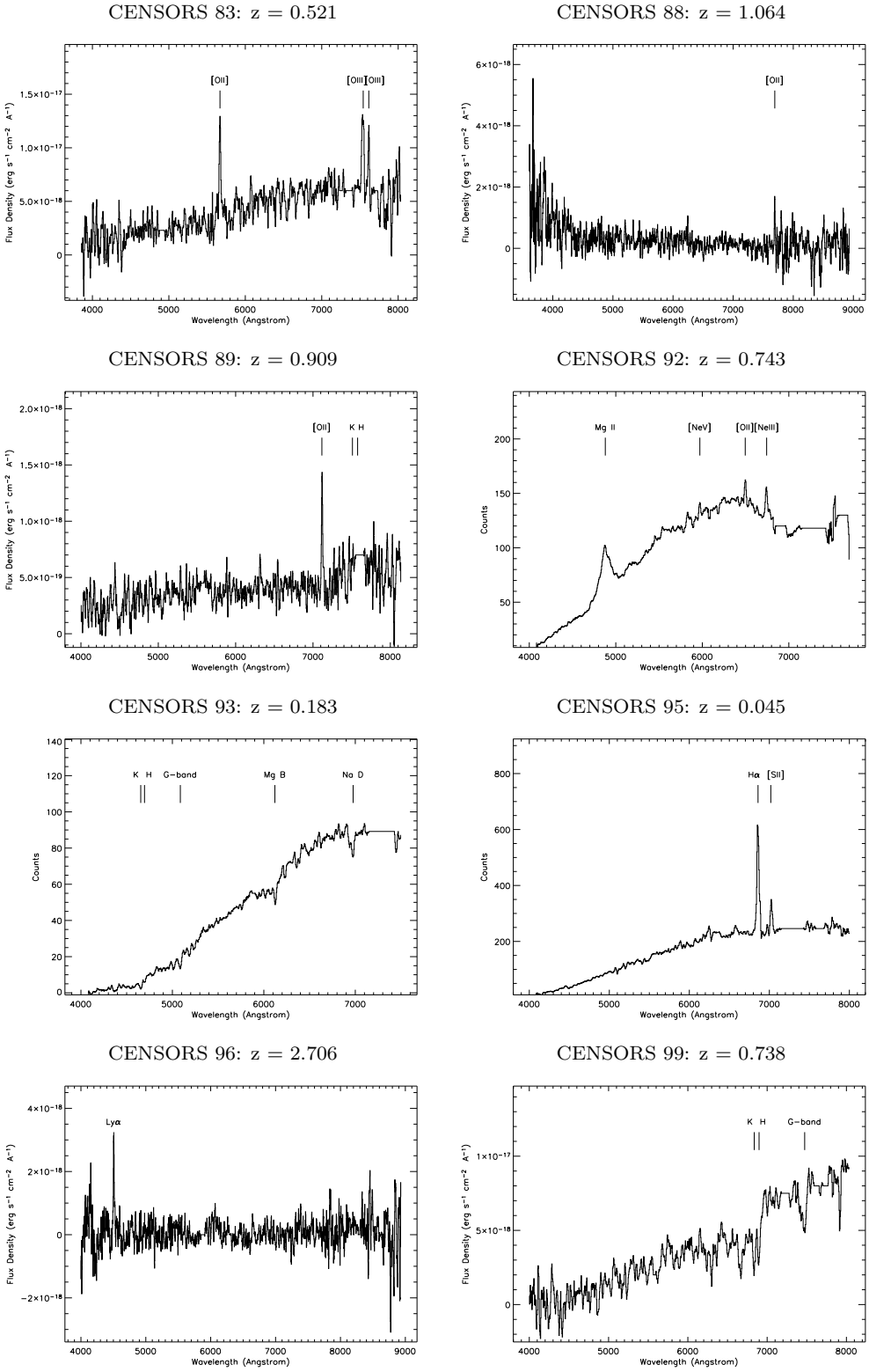

Figure C1. CENSORS spectra with redshift identifications continued.

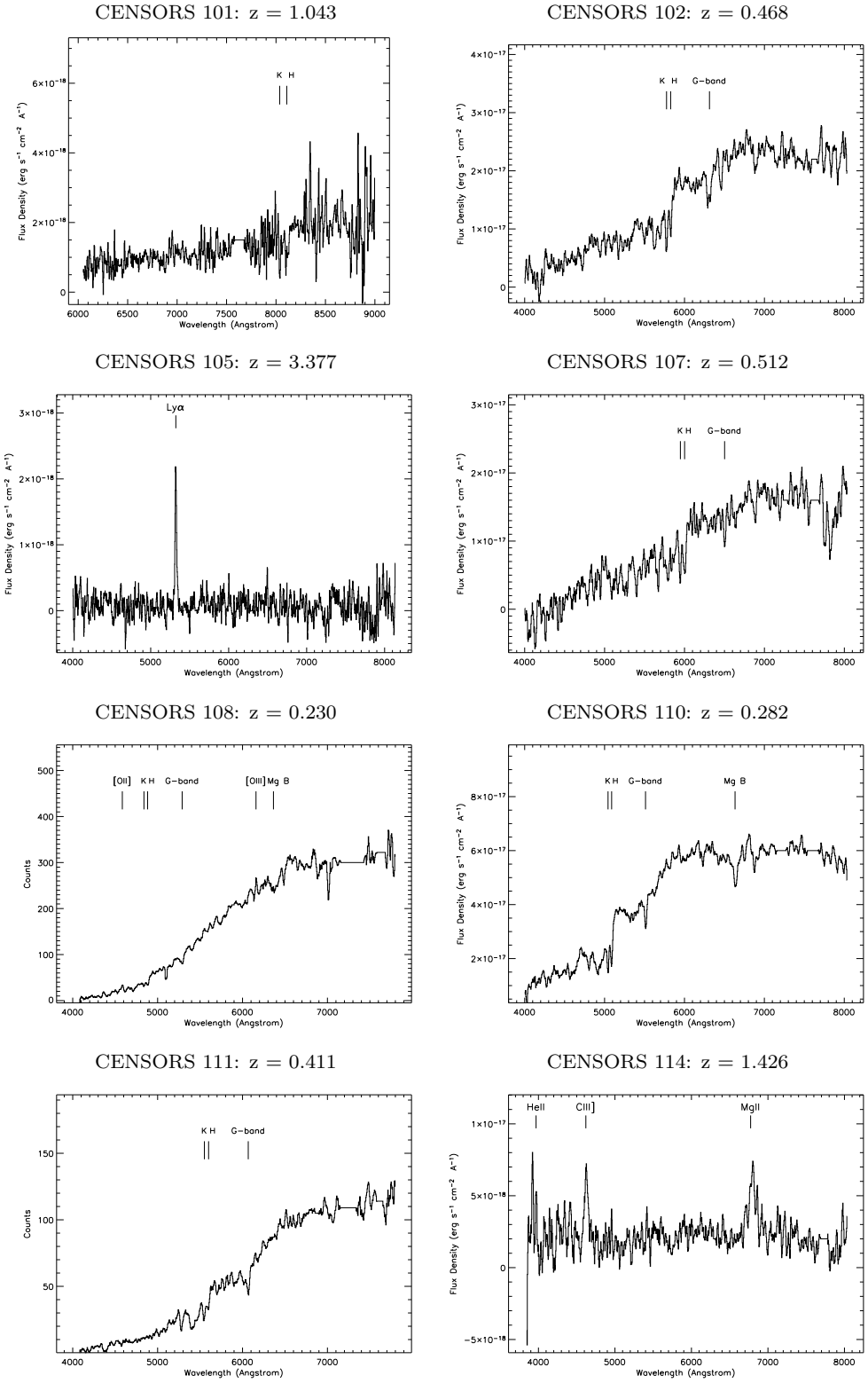

Figure C1. CENSORS spectra with redshift identifications continued.

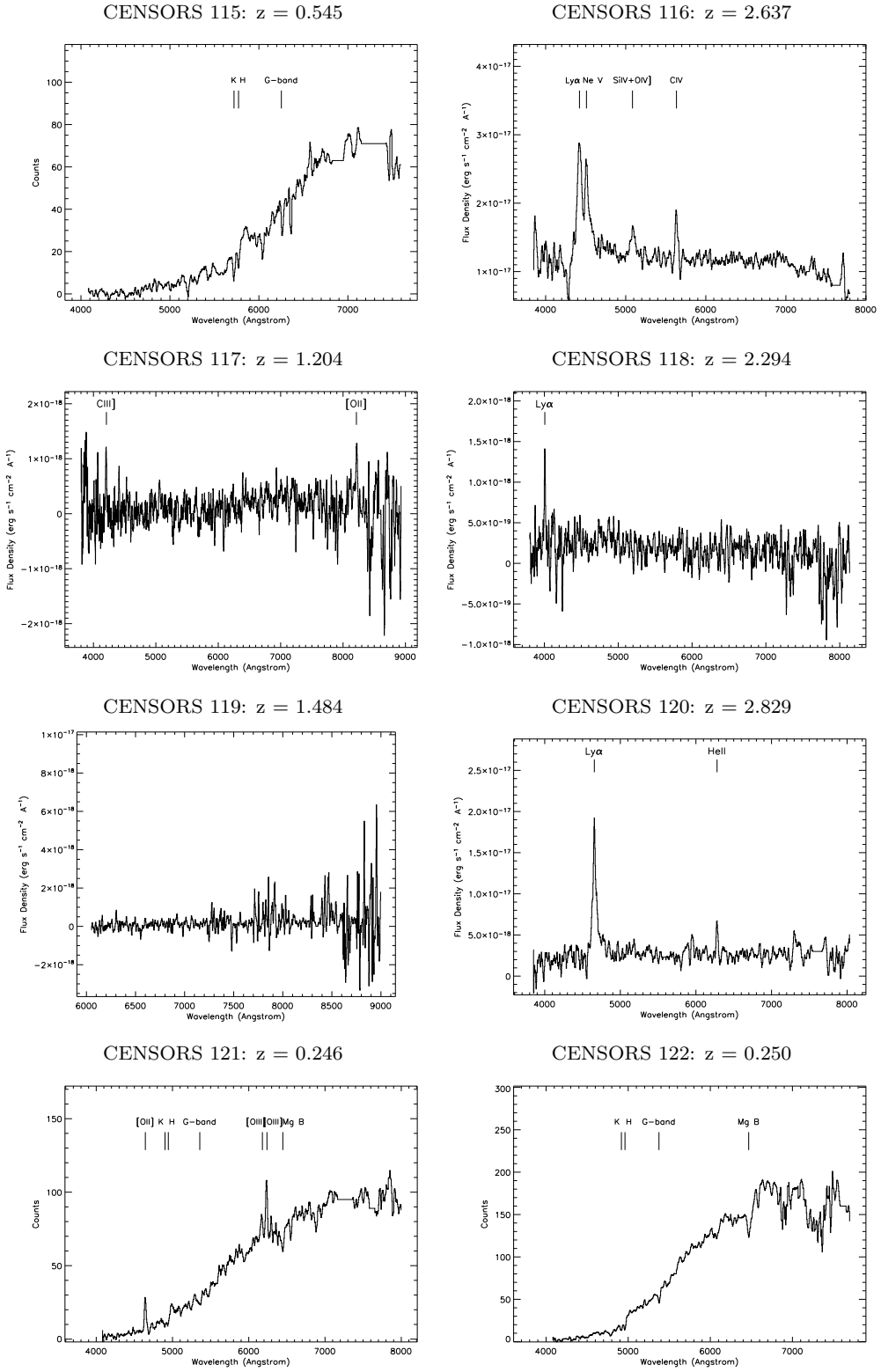

Figure C1. CENSORS spectra with redshift identifications continued.

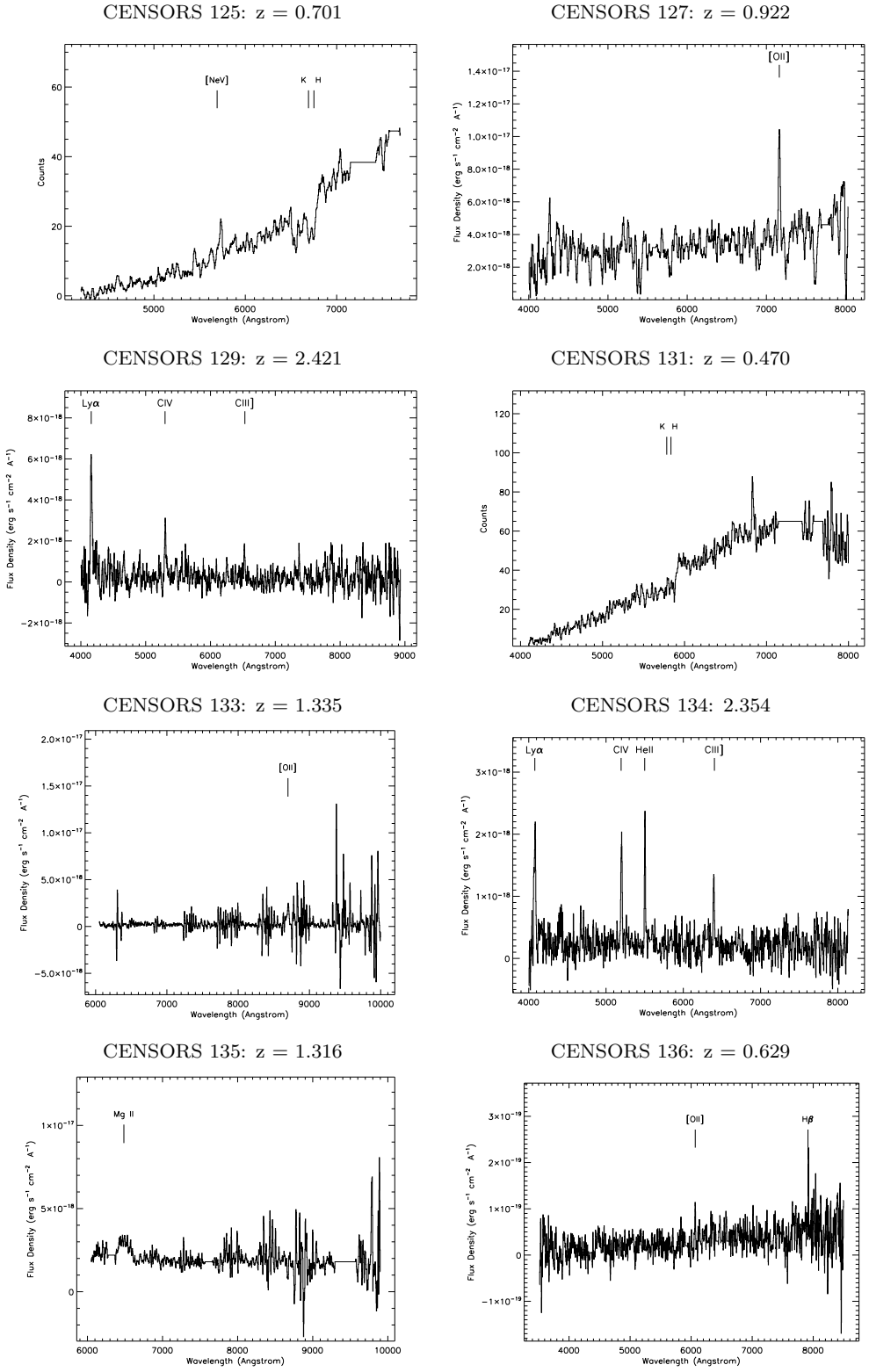

Figure C1. CENSORS spectra with redshift identifications continued.

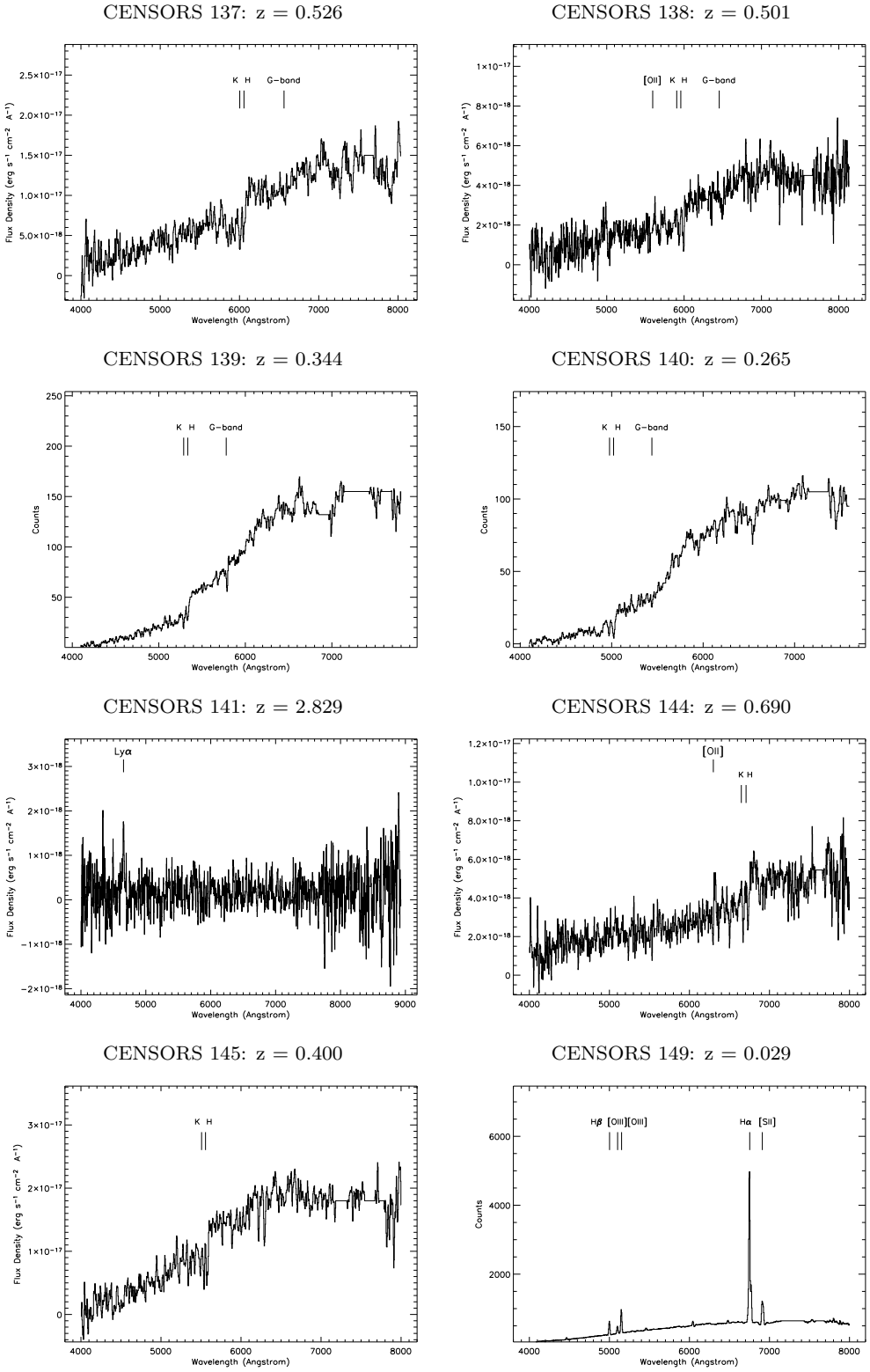

Figure C1. CENSORS spectra with redshift identifications continued.